Geophysical Journal International

Geophys. J. Int. (2017) **208,** 895–917
Advance Access publication 2016 November 10
GJI Geomagnetism, rock magnetism and palaeomagnetism

doi: 10.1093/gji/ggw428

Lamellar magnetism and exchange bias in billion-year-old metamorphic titanohematite with nanoscale ilmenite exsolution lamellae – II: exchange-bias at 5 K after field-free cooling of NRM and after cooling in a +5 T field

Peter Robinson,[1] Suzanne A. McEnroe[2] and Mike Jackson[3]

[1] *Geological Survey of Norway, N-*7491 *Trondheim, Norway*
[2] *Norwegian University of Science and Technology, N-*7491, *Trondheim, Norway. E-mail: Suzanne.mcenroe@ntnu.no*
[3] *Institute of Rock Magnetism, University of Minnesota, Minneapolis, MN* 55455, *USA*

Accepted 2016 November 9. Received 2016 November 6; in original form 2016 June 24

SUMMARY

This is the second of three papers investigating properties of titanohematite-bearing quartzo-feldspathic rocks that create a significant remanent magnetic anomaly in the Modum District, South Norway. The first paper provided initial magnetic results, mineralogical characterization and evidence for the presence of lamellar magnetism. In this paper, knowledge of lamellar magnetic properties is explored through experiments where ilmenite lamellae were magnetized below 57 K, and interact magnetically along interfaces with the titanohematite host. Samples with known NRM directions were placed in specific orientations in an MPMS then cooled in zero field to 5 K, where hysteresis loops were measured in fields up to 5 Tesla. This assured that results were ultimately related to the natural lamellar magnetism produced during cooling ∼1 billion years ago. In a second set of experiments the same oriented samples, were subjected to a +5 Tesla (T) field then field cooled to 5 K before hysteresis experiments. The first experiments consistently produced asymmetric shifted hysteresis loops with two loop separations, one in a positive field and one in a negative field. Without exception, when the NRM was oriented toward the negative field end of the MPMS, the bimodal loop showed a dominant loop separation in a positive field. By contrast, when the NRM was oriented toward the positive field end of the MPMS, the bimodal loop showed a dominant loop separation in a negative field. Both observations are consistent with antiferromagnetic coupling between the hard magnetization of ilmenite and the more easily shifted lamellar magnetism of the hematite. The bimodal nature of the loops indicates that the NRMs are vector sums of natural lamellar moments, which are oriented both positively and negatively, and that these opposite moments control the orientations of ilmenite magnetizations when cooling through 57 K. Here, extreme exchange biases up to 1.68 T were measured. The second set of experiments produced asymmetric shifted hysteresis loops with one opening always in the negative field. These observations indicate that the +5 T field applied at room temperature rotated the hematite lamellar magnetism in a positive direction, so that upon cooling all the ilmenite lamellae acquired negative magnetic moments, thus causing unimodal negatively shifted loops. Here, the largest exchange bias among the unimodal loops was only 0.7 T. These results will be used in paper III to build a better understanding of lamellar magnetism at the atomic layer scale.

Key words: Magnetic and electrical properties; Magnetic mineralogy and petrology; Rock and mineral magnetism; Microstructure.

1 INTRODUCTION

Field studies of amphibolite-facies Mesoproterozoic metamorphic rocks responsible for negative aeromagnetic anomalies in the Modum District, South Norway (McEnroe *et al.* 2016, hereafter referred to as Paper I), led to discoveries of titanohematite samples with unusual magnetic properties caused by nanoscale ilmenite exsolution lamellae with their related lamellar magnetism. Paper I

© The Authors 2016. Published by Oxford University Press on behalf of The Royal Astronomical Society.

focused on a quartz-plagioclase-biotite granulite layer ~3 m thick containing dispersed titanohematite grains with a strong lattice-preferred orientation parallel to a steep regional foliation. When samples with their NRM, produced 1 billion years ago, were cooled in zero field down to 10 K, hysteresis loops run at these temperatures (*T*s) consistently showed bimodal exchange bias caused by magnetic remanence induced within the ilmenite below its T_N (Néel *T*) by antiferromagnetic (AF) coupling with the adjacent lamellar magnetism. By contrast when the same samples, were cooled in a positive magnetic field of 1 Tesla (T), causing a strong unimodal lamellar magnetism, the ilmenite moments, upon passing T_N, adopted a consistent negative orientation, giving rise to unimodal negative exchange bias.

Background on the samples and their general magnetic properties, and electron microprobe analyses (EMP) of the titanohematite are given in Paper I. Experiments at high *T* were made to determine the Néel *T*s and estimated inferred compositions of titanohematite hosts. Experiments at low *T* demonstrated the presence of fine ilmenite exsolution below optical resolution. Their presence was then confirmed by room-*T* and low-*T* Mössbauer spectroscopy, and by transmission electron microscopy (TEM) in dark-field images through the 1 −1 −1 reflection, showing ilmenite lamellae parallel to (001) of hematite with thicknesses ~1.2 to 1.7 nm and aspect ratios 7–13. A theoretical and experimental explanation was also provided concerning a component of room-*T* lamellar magnetism that is out of the (001) plane, thus enabling it to couple with the AF components of ilmenite normal to (001) below T_N of ilmenite.

Here, we discuss the results of a series of low-*T* hysteresis experiments. Paper III presents crystal-magnetic models to explain the origin of the varied exchange bias in these results, including the results of EBSD measurements, and the role of lattice-preferred orientation.

2 GEOMETRY OF MAGNETIC EXPERIMENTS

The conclusions of previous studies on samples here referred to as MOD 2, which showed extreme exchange bias of ~1.3 T (Harrison *et al.* 2007; McEnroe *et al.* 2007a; Fabian *et al.* 2008) and MOD22 (McEnroe *et al.* 2016), relating both to lamellar thickness and to the out-of-plane component of lamellar magnetism, were employed in the design of more sophisticated magnetic experiments. These were initiated using the cryogenic magnetometer at the Institute of Rock Magnetism. There were some doubts concerning the nature of exchange bias created by the NRM, because MOD2 and MOD22 samples showed a predominant positive bimodal bias in the opposite sense from the bias achieved from cooling in a strong positive field.

The Princeton Measurements vibrating sample magnetometer (VSM) and the Quantum Design 'Magnetic Properties Measurement System' (MPMS) are 1-D in their operation: they measure magnetic intensity and apply fields only along one axis, and the vector quantities can be either positive or negative along that one direction. In magnetic experiments made on a randomly oriented set of grains or on a rock without lattice-preferred orientation (LPO), it is assumed that orientation of the sample within the instrument is of little consequence in interpreting the results. Here we show that this is incorrect in experiments on samples with an existing NRM dominated by lamellar moment, and these effects are further enhanced when the sample possesses an LPO. Titanohematite is a phase with a strong magnetocrystalline anisotropy (Robinson *et al.* 2004, 2012) in which the NRM is constrained with respect to the (001) basal plane. If a sample has a strong LPO, consists of several crystals with a similar orientation, or, in the extreme case, consists of a single crystal, then the direction and intensity of magnetization measured will depend heavily on exactly how the sample is placed in the instrument, both with respect to the NRM, and with respect to the LPO.

The placement concept was illustrated in fig. 9 of McEnroe *et al.* (2007b), showing two very different magnetic hysteresis loops, run on the same small polished hemo-ilmenite sample, and under the same room-*T* conditions. That sample, from Allard Lake, Quebec, showed traces of (001) exsolution lamellae on the polished surface. Hysteresis loops were measured on a VSM in two orientations, one with the lamellar traces quasi-parallel to the instrument field, the other with lamellar traces quasi- normal to the field. In the orientation parallel to the lamellar traces, where remanence intensity was stronger, the bulk coercivity was weaker at 137 mT. In the orientation normal to lamellar traces, where remanence intensity was weaker, the bulk coercivity was much stronger at 343 mT.

From the above discussion, it is obvious that single-axis magnetic experiments conducted on grains with the NRM mounted at random will provide no concrete information on the effect of NRM orientation on features of low-*T* hysteresis loops, and most especially the effect of such orientation on whether a dominantly positive or negative exchange bias will be observed. Rather than continuing to resort to luck to learn about NRM orientation, a method needed to be found by which the NRM orientation of individual grains could be determined accurately, to allow optimal orientation of the specimen in the single-axis magnetometer for later low-*T* experiments. At the same time it was important to develop preliminary theoretical models connecting features of lamellar magnetism and ilmenite magnetism at low-*T*, with orientation in the instrument.

3 OPTIMAL CRYSTAL ORIENTATION FOR MEASURING LOW-*T* EXCHANGE BIAS

Here we look at how to measure the net magnetization resulting at low-*T* when there are two magnetizations to consider, both the lamellar magnetism inherent at room-*T* and the ilmenite magnetism at low-*T*. In principle, the best measurement direction would be the direction of the vector sum of the two different magnetizations. This requires an acceptable magnetic model, which is attempted in the block models in Fig. 1, based on the proposed nature of low-*T* magnetic coupling between hematite and ilmenite explained in Paper I, fig. 9.

The two phases in each of the four models in Fig. 1 are assumed to belong to a single crystal and each contains 10 cation layers. The central layer in each block is an Fe^{2+} layer in the center of an ilmenite lamella, which also contains two black Ti layers. TEM data given in Paper I indicates that typical lamellae in the MOD22 sample are ~1.2–1.7 Å thick which would correspond to 3 Ti layers and 2 Fe layers to 5 Ti layers and 3 Fe layers, respectively. The lamellae are likely disk-shaped (Kasama *et al.* 2009) and our TEM information indicates disk diameters 8.4–22 Å and aspect ratios of 7–13. Monte Carlo modeling of exchange bias by Harrison *et al.* (2007) showed that with an even number of Fe layers, for example 3 Ti and 2 Fe, there is no net ilmenite magnetization and no exchange bias occurs. With an odd number of Fe layers, for example 5 Ti and 3 Fe, there is a net ilmenite magnetization conducive to exchange bias. It is true that an ilmenite layer, as in Fig. 1, with only 2 Ti and 1 Fe layer, does also have a net magnetic moment conducive to

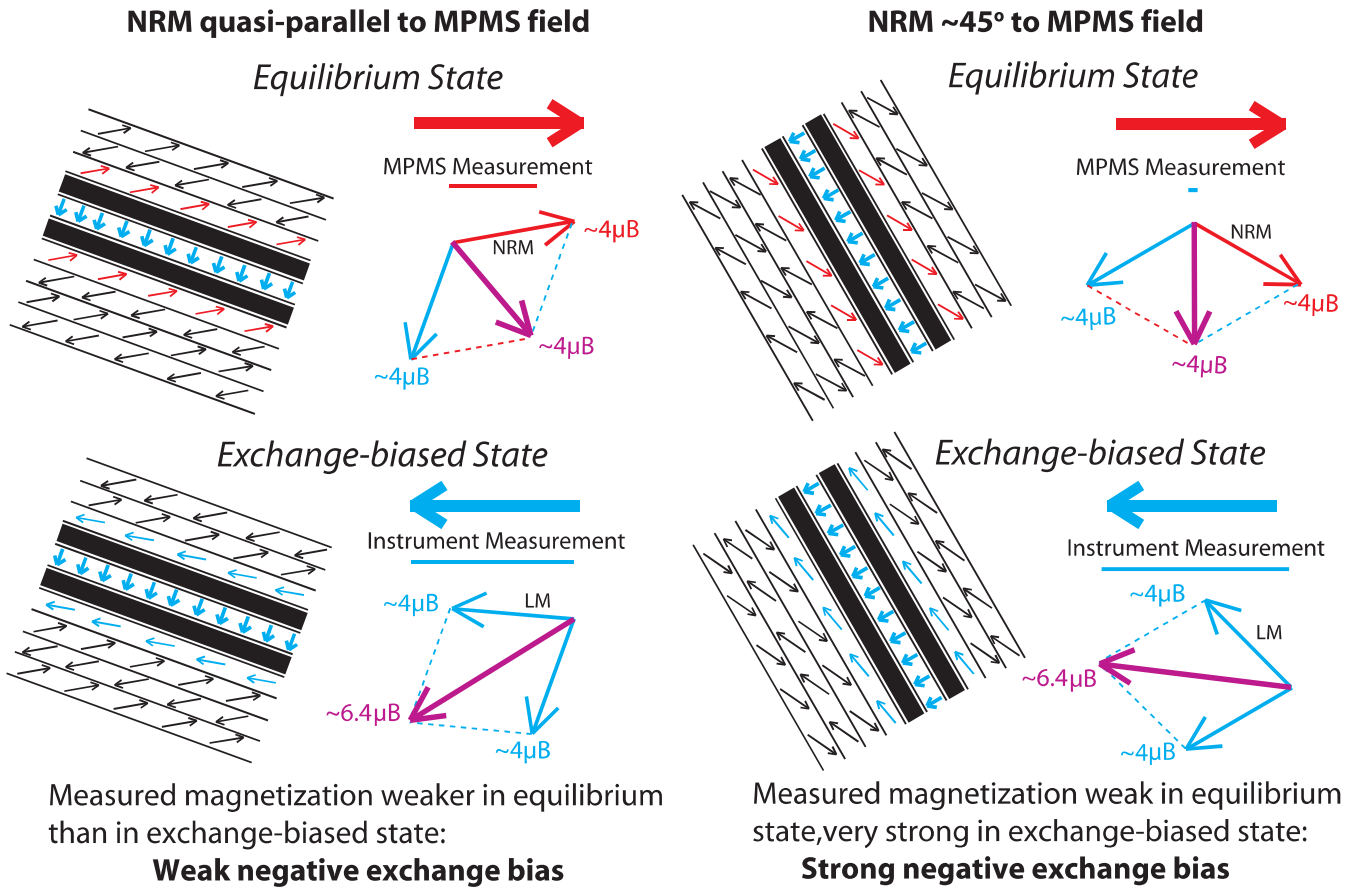

Figure 1. Theoretical diagram of lamellar magnetic moments and ilmenite magnetic moments below T_N of ilmenite in two different crystal orientations in a single-axis MPMS, resulting in records of weak and strong negative magnetic exchange bias. Note that lamellar moments in the exchange-biased state, according to theory, are at a smaller angle to (001) than in the equilibrium state.

exchange bias, but unlike the version with 5Ti and 3 Fe layers, there is no magnetic interaction between Fe layers internal to ilmenite to hold that magnetization, therefore the only interaction would be with adjacent hematite contact layers. Thus, the model ilmenite used in Fig. 1 is a space-saving illustrative convenience, where a model with 3 Fe layers would be more correct, though either would show a net ilmenite magnetization equivalent to that of a single Fe layer.

The Monte-Carlo modeling (Harrison *et al.* 2007) required the use of a very small number of atoms hence the model ilmenite lamella with 3 internal Fe layers had an aspect ratio <1 compared to our measured 7–13. This had the effect of emphasizing interactions on the edges of lamellae, which necessarily would be less important in lamellae with a high aspect ratio. The modeling also showed that the position of the lamellar magnetism with changing fields cannot be correctly tracked in two-dimensions as in Fig. 1. Harrison *et al.* (2007) showed that it generally follows 3-D paths.

Outside of the two Ti layers in Fig. 1 are the two 'contact layers' of lamellar magnetism. Both the contact layers and the hematite layers are shown with their magnetic moments tilted out of the basal plane by about 30° as demonstrated by Harrison *et al.* (2010). A key and unexpected result of that study was to show that the tilting is present at room-*T* and must have been present under conditions of acquisition of lamellar magnetism. This provides the necessary and logical means, as illustrated in Paper I, fig. 9, by which the lamellar moment can influence the ilmenite magnetization, which would be impossible if the two moments were exactly normal to each other. In the Harrison *et al.* (2007) model, the tilting of the lamellar moment is shown as continuing out into surrounding hematite layers, and that is also shown here. Exactly how far is not known certainly. Also note that the number of hematite layers on opposite sides of the ilmenite lamella is not the same. This is because the number of hematite layers in the block must be odd (Robinson *et al.* 2004), so that top and bottoms of the blocks have opposite moments, allowing them to be assembled into a single magnetized hematite host.

The hematite host contains a lamellar NRM acquired above T_N of ilmenite, which is at 30° to the hematite basal plane (001). Because we are concerned with the vector sums of lamellar magnetism and ilmenite magnetism from cooling below ilmenite T_N, all of the blocks in Fig. 1 are completely magnetized, so the ilmenite has a remanence direction normal to (001) determined by the contact layer remanence direction when passing through ilmenite T_N. In 'equilibrium states' in zero field, in the upper half of the figure, the lamellar magnetism, indicated by small red arrows pointing generally to the right, has caused the ilmenite magnetism, indicated by small blue arrows, to point in the opposite direction and uniformly downward to the left. In the 'exchange-biased states' produced by strong applied fields, in the lower half of the figure, the 'hard' ilmenite magnetizations remain unchanged, but the application of a strong negative field has caused the lamellar magnetism, as well as the associated hematite magnetic moments to reverse. This state violates the normal AF coupling between the ilmenite Fe layer and the contact layers, and only is reached in a strong negative field. There is theoretical

evidence (Harrison *et al.* 2007) that in the exchange-biased states, the tilt angle of the lamellar moments out of the (001) basal planes will be smaller than in the equilibrium states, that will have an effect on the net magnetic moment in the instrument direction.

The next consideration is the effect of sample orientation of single-crystal material in the instrument on the resulting measured magnetic exchange bias. This involves measuring the sensor-parallel component of the vector sum (violet arrows) of the lamellar NRM's, shown with red arrows when positive and blue arrows when reversed, and ilmenite moments shown as blue reversed throughout.

Each model crystal in Fig. 1 has been oriented in the MPMS with the direction of the lamellar NRM either quasi-parallel or at ~45° to the MPMS field axis. In the quasi-parallel orientation in Fig. 1(left-hand panel), in zero field, after reaching below T_N of ilmenite, in the so-called 'equilibrium state', the vector sums of the red and blue arrows will point down to the right, and the measured intensity in the instrument direction will be approximately 75 per cent of the original NRM. Upon application of a strong negative field, reaching the 'exchange-biased state', the vector sum of both blue arrows will be longer and down to the left, and the measured intensity in the instrument direction will be about 130 per cent of the reversed NRM, and the result will be a weak negative exchange bias (i.e. hysteresis loops will be asymmetrically more open in negative fields).

In the ~45° orientation in Fig. 1(right-hand panel), in zero field below T_N of ilmenite, in the 'equilibrium state', the vector sum of the red and blue arrows will point almost vertically down (i.e. perpendicular to the sensor axis) and slightly to the right, and the measured intensity in the instrument direction will be approximately 5 per cent of the original NRM intensity in the opposite direction. Upon application of a strong negative field, reaching the 'exchange-biased state', the vector sum of both blue arrows will be longer and horizontally to the left, and the measured intensity in the instrument direction will be about 200 per cent of the reversed NRM measured in that direction. The measured magnetization is significantly weaker in the equilibrium state than in the exchange-biased state and a strong negative exchange bias is observed.

If the natural material fulfills the concepts illustrated in Fig. 1, we can see that the most significant measurements of low-temperature magnetic exchange bias will be obtained by placing the specimen in the MPMS with the NRM ~45° to the field axis. Here we have the additional option of placing the sample with the positive NRM toward the positive direction of the instrument or toward the negative direction. The predictive models in Fig. 1 assume a more or less equal strength of lamellar magnetism and ilmenite magnetism. If the net lamellar magnetism has a much larger intensity than the net ilmenite magnetism, as we now suspect from the new experiments here, the vector sums will be different than inferred in Fig. 1 and

Table 1. Measured NRM orientations and intensities of candidate grains for NRM cooling experiments. Samples run 2010 in bold, 2013 in bold italics.

Sample, piece, fig. no.	NRM ∧ +z axis[a]	Placement	Moment Am[b]	Wt. (g)	Intensity[b] ($Am^2\ kg^{-1}$)
MOD22-5, C1 S3I	**+43.4**	**1**	**2.597E-07**	**0.0399**	**6.509E-03**
MOD22-5, C2 3F	**137.4 (−42.6)**	**2**	**4.649E-07**	**0.039**	**1.192E-02**
MOD22-5, C3	149.8 (–30.2)		4.016E-07		
MOD22-5, C4	+33.7		1.996E-07		
MOD22-5, C5 3D	***+71.8***	***3***	***3.446E-07***	***0.019***	***1.814E-02***
MOD22-6, C1 S3C	***+71.8***	***3***	***1.509E-06***	***0.0579***	***2.606E-02***
MOD22-6, C2 3G	**144.9 (−35.1)**	**2**	**1.791E-06**	**0.0397**	**4.511E-02**
MOD22-6, C3 3A	**+48.3**	**3**	**1.550E-06**	**0.0578**	**2.682E-02**
MOD22-6, C4	115.2 (−64.8)		6.168E-07		
MOD22-6, C5	+30.3		4.670E-07		
MOD22-8a, C1	154.5 (−25.5)		4.755E-07		
MOD22-8a, C2 S3J	***+54.8***	***1***	***3.933E-07***	***0.0391***	***1.006E-02***
MOD22-8a, C3	+16.5		2.901E-07		
MOD22-8a, C4	+15.5		3.850E-07		
MOD22-8a, C5 S3E	**168.6 (–11.4)**	**4**	**5.321E-07**	**0.0365**	**1.458E-02**
MOD22-21b, C1	+65.5		4.426E-07		
MOD22-21b, C2 3H	***+76.6***	***1***	***5.212E-07***	***0.0195***	***2.673E-02***
MOD22-21b, C3	−74.2		1.110E-07		
MOD22-21b, C4 3B	***153.0 (–27.0)***	***4***	***2.369E-07***	***0.0358***	***6.618E-03***
MOD22-21b, C5	+75.6		1.976E-07		

Notes. [a]The angle that the NRM orientation makes with the positive *z* axis of the sample mount, before placing in the MPMS. Where angle was obtuse, equivalent acute angle to –*z* is also given.

[b]Weight-normalized intensities are misleading because grains are not pure oxide, but also contain substantial low-density quartz and feldspar.

Placement details:

1: The +*z* axis of the sample mount was placed toward the positive end of the MPMS. Thus the NRM direction, at an acute angle to the +*z* axis, projected a **positive** component along the MPMS axis.

2: The +*z* axis of the sample mount was placed toward the negative end of the MPMS. Thus the NRM direction, at an obtuse angle to the +*z* axis, projected a **positive** component along the MPMS axis.

3: The +*z* axis of the sample mount was placed toward the negative end of the MPMS. Thus the NRM direction, at an acute angle to the +*z* axis, projected a **negative** component along the MPMS axis.

4: The +*z* axis of the sample mount was placed toward the positive end of the MPMS. Thus the NRM direction, at an obtuse angle to the +*z* axis, projected a **negative** component along the MPMS axis.

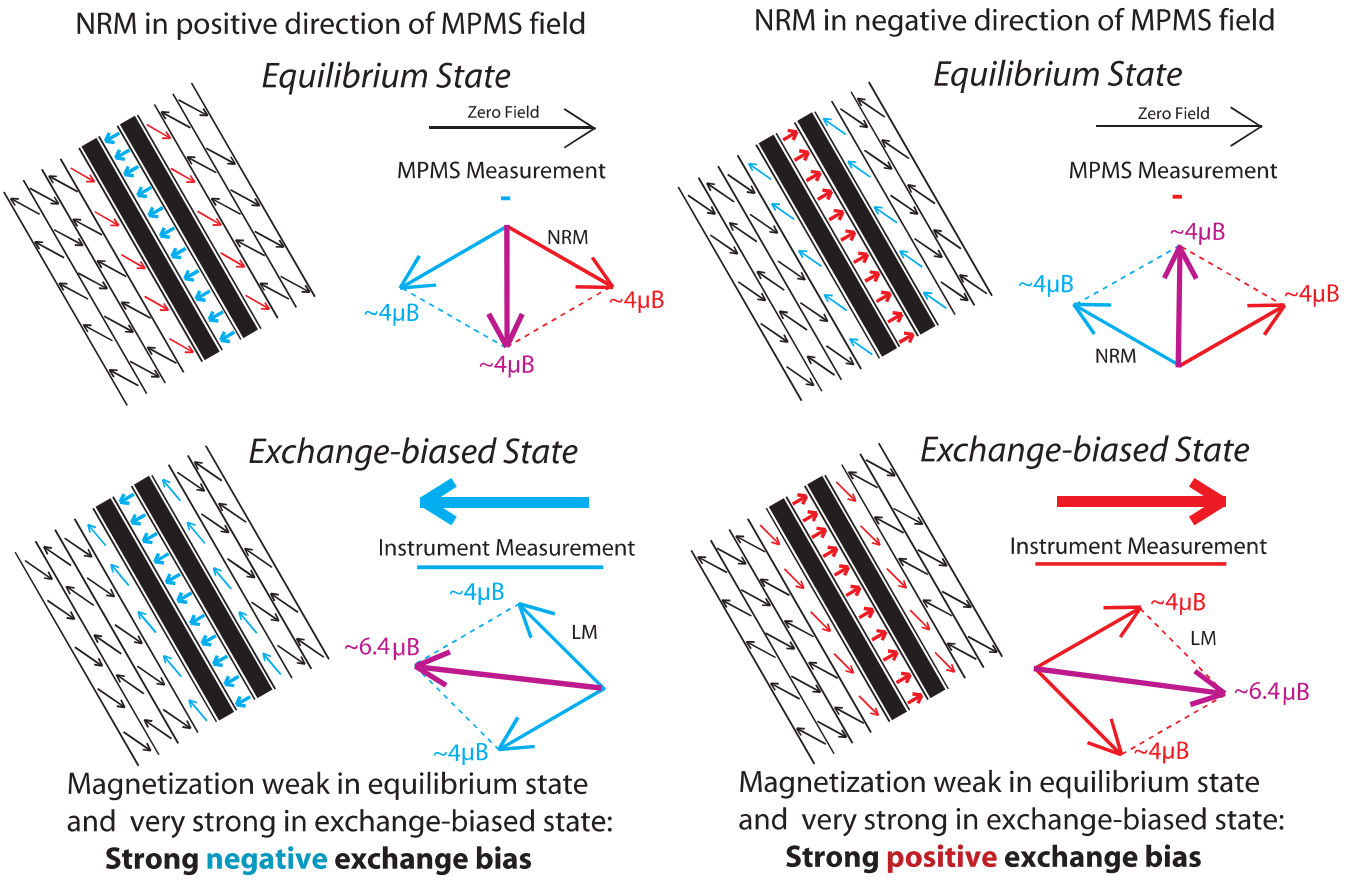

Figure 2. Theoretical diagram to illustrate the separate effects of opposite orientations of the NRM of lamellar magnetism in titanohematite in a single-axis magnetic MPMS leading to bimodal low-*T* magnetic exchange bias in MOD22 samples. Note that lamellar moments in the exchange-biased state, according to theory, are at a smaller angle to (001) than in the equilibrium state.

so will the optimal positions for observing exchange bias. The relationships in Fig. 1 are thus provisional, pending experimental results and more comprehensive modeling.

4 NRM ORIENTATION

The orientation and the intensity of the NRM were measured using a 3-axis cryogenic magnetometer (2 G model 760 with RF SQUIDs). This did not remove all randomness because there was no way to select grains visually for mounting in the MPMS, so several grains from each sample were mounted in arbitrary fixed orientations in gel caps. These were referred to as candidate grains. The cylindrical gel-cap shape defines a unique axis, designated *z*, one end of which was arbitrarily defined to be the positive *z* axis. NRM orientations and intensities were determined on the cryogenic magnetometer for 20 grains from four different samples, Mod 22–5, 22–6, 22–8a and 22–21b. Based on NRM intensity, and other perceived criteria, 10 grains in two groups of 5 were selected for the next steps of investigation (Table 1). Once the NRM orientation was determined relative to the +*z*-axis of the gel-cap sample mount, it was possible to place the sample mount co-axially in either direction relative to the magnetic axis of the MPMS. The footnotes in Table 1 explain the instrument placement used for each gel-cap sample and each of the hysteresis diagrams has an inset illustrating how this was accomplished.

5 THEORY CONCERNING EXCHANGE BIAS FROM COOLING AN ORIENTED NRM

The logic for bimodal exchange bias is illustrated in Fig. 2. When a crystal has its NRM vector oriented ~45° to the positive field direction of the MPMS, this will result in a negative exchange bias. Conversely when a crystal has its NRM vector oriented ~45° to the negative field direction of the MPMS, this will result in a positive exchange bias. Crystals containing regions with positively directed NRMs and other regions with negatively directed NRMs could thus be expected to show bimodal exchange bias. The same is true for variously oriented collections of crystals within rock samples.

The origin of this bimodality comes in part from the nature of lamellar magnetism in a titanohematite host and the orientation of the (001) basal plane with respect to the ancient magnetizing field (Robinson *et al.* 2002, 2004, 2012). When the basal plane is not parallel to the magnetizing field, then not all ilmenite lamellae and contact layers will be forced to be magnetically 'in-phase', that is they will not necessarily be separated by odd numbers of hematite layers, which would ensure that the contact layers all had mutually parallel magnetizations. 'Out-of-phase' lamellae (with essentially reversed NRMs) then can lead to bimodal exchange bias. The 'out-of-phase' lamellae were directly observed by Kasama *et al.* (2009) in a hemo-ilmenite grain using Lorentz polarization observations in a TEM. In natural samples with scattered small crystals, it is so far not easy to distinguish between out-of-phase lamellae within

crystals and scattered crystals each magnetized differently, but it appears necessary to investigate both possibilities. We do this in the magnetic models developed in Paper III of this series.

Fig. 2 shows the theoretical results from placing an oriented NRM toward the positive field direction of the MPMS (left-hand panel) or toward the negative field direction (right-hand panel). In both examples the NRM is oriented ∼45° from the field direction of the MPMS to measure predicted maximal exchange bias, explained earlier (Fig. 1), though we know this is an oversimplification.

With positive orientation of the NRM (small red arrows, Fig. 2 upper left), the ilmenite magnetizes negatively (blue arrows) to give the 'equilibrium state'. The violet vector sum of red and blue arrows points almost straight down (i.e. perpendicular to the field axis) and the net magnetization measured in the field direction of the MPMS is negative and very small. In the exchange-biased state in a strong negative field (Fig. 2 lower left), the violet vector sum of all the blue arrows is horizontal and large, so that net magnetization in the field direction of the MPMS is very large, thus yielding a strong negative exchange bias. This is a slight oversimplification because the neutron experiments and related theory by Harrison *et al.* (2010) suggest a smaller tilt angle of the lamellar moments out of the basal plane in the exchange-biased state than in the equilibrium state, thus influencing the net lamellar moment.

With negative orientation of the NRM (small blue arrows, Fig. 2 upper right), the ilmenite magnetizes positively (red arrows) to give the 'equilibrium state'. The violet vector sum of red and blue arrows points almost straight up and slightly to the right and the net magnetization measured in the field direction of the MPMS is very small and positive. In the exchange-biased state in a strong positive field (Fig. 2 lower right), the vector sum of the red arrows is horizontal to the right and large, so that net magnetization in the field direction of the MPMS is very large, thus yielding a strong positive exchange bias. An important caveat related to the models in Fig. 2, is that they only illustrate the potential intensity of ilmenite magnetization coupled to adjacent contact layers that is involved in exchange bias. They may not at all accurately predict the total of ilmenite moments in thicker lamellae.

Expected results from cooling an NRM below T_N of ilmenite followed by a low-*T* hysteresis measurement would be: (1) a dominantly negative exchange bias if the NRM is placed toward the positive field direction of the MPMS, or (2) a dominantly positive exchange bias if the NRM is placed toward the negative field direction of the MPMS.

The properties of candidate grains are shown in Table 1. In the first group of five (I, F, G, A and E), four had favorable NRM orientations 35–48°, and good intensities 7–45 mAm^2 kg^{-1}. Candidate grain E in one sample had a less favorable angle of 11°, useful to test the rules, but had the largest intensity in that sample. In a second group of five (D, C, J, H and B), D, C and H had very large angles between 71° and 77°, J had an intermediate angle of 55° and B a small angle of 27°. Intensities were similar 7–27 mAm^2 kg^{-1}.

5.1 Importance of NRM$_Z$

The measured NRM directions and intensities of the Mod 22 samples represent a composite of all the crystals in each sample and the composite directions and intensities of the individual exsolution lamellae within all the crystals. Such a condition is different from the single lamellar models used in Figs 1 and 2 to design and understand arrangements for the hysteresis experiments.

The intensities of the NRMs depend on the amount of magnetic material in the samples, and on the vector sum of the NRMs in the sample. These are rock samples, not mineral samples, and are dominated by silicates. The rocks appear to have been originally detrital sedimentary rocks, with irregular distributions of detrital grains. Thus, individual pieces from the same core sample may have different populations of detrital magnetic minerals reacted and recrystallized under upper amphibolite-facies conditions.

For hysteresis experiments, the total NRM intensity is less important than the NRM moment intensity measured along the field axis of the MPMS, as illustrated in the insets in Figs 3 (a) and (b) (also S3A–S3J). We designate this moment, either positive or negative along the instrument, as NRM$_Z$. This intensity is a function of the total NRM intensity combined with the angle θ that the NRM makes with the field axis. For a constant total NRM intensity, NRM$_Z$ is an inverse function of θ where NRM$_Z$ = NRM cos θ, ranging from full NRM at $\theta = 0°$ to 0 at $\theta = 90°$. These relationships are explored in Table 2, showing the full NRM intensities measured on the cryogenic magnetometer, the calculated NRM$_Z$ from this, and the NRM$_Z$ measured on the MPMS (columns 1, 3 and 4).

Our sample G, with by far the largest total NRM intensity at 0.045112 Am^2 kg^{-1}, also has the largest value of NRM$_Z$ at 0.03390, and this also has a small angle θ at +35°. By contrast, sample C, with the third largest total NRM intensity at 0.026064 Am^2 kg^{-1}, has a low NRM$_Z$ at -0.00782 at Am^2 kg^{-1}, but that is because of its large angle θ at –71.8°. It is the NRM intensity along the field direction of the MPMS recorded at room *T*, that largely determines what is recorded in the low-temperature hysteresis experiments controlled by ilmenite magnetization produced by AF coupling across lamellar interfaces on cooling below T_N.

6 RESULTS OF EXPERIMENTS AT 5 K

6.1 General features of low-*T* hysteresis loops

Experiment results on 10 candidate grains (A–J) are shown in hysteresis loops in Figs 3(a) (A, B, D) and (b) (F, G, H) and for all samples in an electronic supplement (Figs S3A–S3J). Loops were measured in a 5 T field. The parts of Fig. 3 labeled NRM resulted after a lamellar NRM, acquired about 1 billion years ago, was cooled in zero field to 5 K, before applying any experimental magnetic field. Because of the influence of the initial NRM orientation, we refer to these as 'NRM loops' following McEnroe *et al.* (2016). The parts of the figure labeled FC resulted after the same sample, in the same orientation, was returned to room *T*, a field of +5 T was applied and the sample field-cooled (FC) to 5 K before running the hysteresis loop. An icon in upper left corner of each NRM loop in the figures shows how the NRM, already fixed in a gel cap, was oriented in the MPMS before cooling.

Below each of the 12 loops in Fig. 3 (20 loops in Figs S3A–S3J) measurement of the loop separation size is shown in shaded gray, as expressed on plots 'Mrh', as illustrated in Fig. 4. With the 'Mrh' method, an average of upper and lower loop positions, weight-normalized to Am^2 kg^{-1}, is taken and this is plotted against the upper loop position. The height of the upper loop plotted against the average is exactly half the true loop separation. Based on this, the gray shaded loop separations are plotted with a factor x5 compared to the vertical scales. The 20 Mrh curves are in the electronic supplement, with vertical scales adjusted to the largest loop separation. They are the key to numerical values given in Tables 3–8.

Previous NRM loops run on MOD2 and MOD22 were bimodal with predominant positive exchange bias, and we were concerned why this should be so. By contrast FC loops and one ZFC loop

after imposition of a positive IRM, showed predominant negative exchange bias. The first three new runs on pre-oriented samples all showed predominant negative exchange bias, and a positive exchange bias was only measured in the fourth run, and several subsequent runs, confirming for the first time that the sign of the equilibrium-state lamellar moment as inserted in the MPMS determines the dominant exchange bias. This key result is emphasized here and repetition is avoided in what follows.

The results of all ten sets of loops are summarized in Tables 3–7, here in two groups according to whether the dominant observed NRM exchange bias is negative or positive. The first columns in these tables show sample and figure number, acute angle of the NRM with respect to the negative or positive instrument axis and NRM and FC labels.

6.2 Loop closure at high fields and the question of saturation

The positions of loop closures in positive and negative fields (Table 3) were estimated by: (1) Direct observation of the plotted loops. (2) Study of the 'Mrh' curves (Fig. 4 and electronic supplement Figs S4A–S4J) where closure of a loop would be indicated when the value of Mrh (half the loop separation height) reaches zero. When the magnetizations are small and the fields large, some of the 'Mrh' curves pass through zero more than once. These results are probably related to minor problems with thermal equilibrium at these low *T*s and high fields. In Table 3 one can see that these problems are more common in high positive fields at the beginnings of the hysteresis runs. The results for each method are listed to illustrate the problems without trying to track down the individual causes.

With any hysteresis loop there is always the question of determining the points at which magnetic saturation is reached, assuming it is reached at all. This is a problem here, partly because the sources of magnetization at very low temperature, lamellar magnetism and the magnetism of quasi-antiferromagnetic ilmenite are both involved. It appears that lamellar magnetism may be oriented to a common direction in fields close to 5 T, reorienting the hematite host, and also overcoming AF coupling to the adjacent ilmenite. By contrast, internally to ilmenite, the magnetization would increase parallel to the field, moving moments out of perfect antiparallelism, but never overcoming the AF coupling that would lead to the metamagnetic state at ~10 T (Kato *et al.* 1982). Saturated magnetization (Ms) was estimated by laying tangent lines as close as possible along upper limbs at +5 T and lower limbs –5 T, then measuring the vertical intercepts on the zero-field axis. Results were hard to interpret and not recorded here.

6.3 Tesla positions of loop separations and loop separation sizes

Table 4 shows the values in T for the maximum separation (peak) positions of the loops, the values in $Am^2\ kg^{-1}$ for the maximum separation (peak) heights of the loops, and the values in $J\ kg^{-1}$ for the separation (peak) areas of the loops (columns 1, 2 3). For each NRM loop, with bimodal hysteresis, the larger field value for a maximum separation peak, the larger maximum separation peak height, and the larger separation peak area, are shown in bold.

Table 4 shows that samples placed in the MPMS with NRM_z placed negatively (A–E) had NRM loops with a predominant positive maximum separation (peak) height and exchange bias, and all placed with NRM_z placed positively (F-J) gave a predominant negative maximum separation (peak) height and exchange bias. In addition, with the exception of A and H, all peaks with the smaller maximum separation (peak) height had a larger hysteresis shift, either positive or negative, away from the origin. Also, without exception, the negative unimodal shifts of the FC loops were numerically much smaller than either of the two bimodal shifts in the corresponding NRM loops. By contrast, in comparing to total areas of the loops (see Table 7) the areas of the FC loops are consistently larger than the areas of the NRM loops, with the sole exception of J.

In the bimodal NRM loops, the relative maximum separation (peak) heights are compared by using the percentages of each peak height with respect to the sum of the two heights. The larger peak heights range from 59.3 to 53.6 per cent, except for the most asymmetric bimodal loops, 3A at 68.8 per cent and 3 G at 73.1 per cent. The smaller peak heights range from 46.2 per cent to 40.7 per cent except for 3A at 31.2 per cent and G at 26.9 per cent. Typically, then, the natural lamellar magnetism created in response to the relatively weak Earth field under high-temperature exsolution conditions with thermal fluctuations, is relatively weak compared to its theoretical potential, and is reflected in the generally small deviations from 50 per cent that would indicate no field effect at all. Similar percentages can be used to compare loop separation areas, with similar results, with exceptions 3 G and 3 J, where the area measurement for 3 J using Mrh is compromised by relations at high fields. Considering the wide variety of placement angles to the field direction of the MPMS from –11 through 90 to +32, it is notable that most of the NRM loops show loop separation percentages quite close to 50 per cent.

6.4 Shape of hysteresis loops and hardness of ilmenite magnetization

There are several ways to look at hysteresis loop shape beyond the details of asymmetric loop separations. These help to understand how 'tall' the loop looks overall relative to the asymmetric remanence recorded in the middle. Some of the loops are very 'squat' where remanence plays a dominant role. Others are 'tall' where induced magnetization may be more important. Parameters that control these features are the intercepts of the loops at –5 T and +5 T, the values of remanence Mr– and Mr+ at zero field, and the values of the average Mr (Mr_{AV}). These parameters and numbers derived from them are listed in Table 5.

Generally, the induced magnetization towards –5 T and +5 T can be considered to have four possible components: (1) The linear effect of increased field on paramagnetic ions; (2) The effect of increased field strength on lamellar magnetism caused by reorientation of magnetic moments; (3) The essentially linear effect of increased field in re-orienting the magnetic moments of quasi-AF hematite and ilmenite and (4) The effect of magnetite reaching saturation at low fields. The last is shown with prominence in the loops in Fig. 3H, where the presence of a trace amount of magnetite is confirmed by a Verwey transition in cooling and warming curves (see Section 7), but appears to be unimportant in other loops.

In general, if the values of the intercepts at 5 T are both large and similar, and the values of Mr are close together, the field-induced magnetization is much larger than the remanence, and the loop is 'tall'. Conversely, if the intercept values are both smaller and closer to the Mr values, then the loop can be described as 'squat'. Visually it is easy to sort the loops into 'tall': A, E, G, H, I and J, and

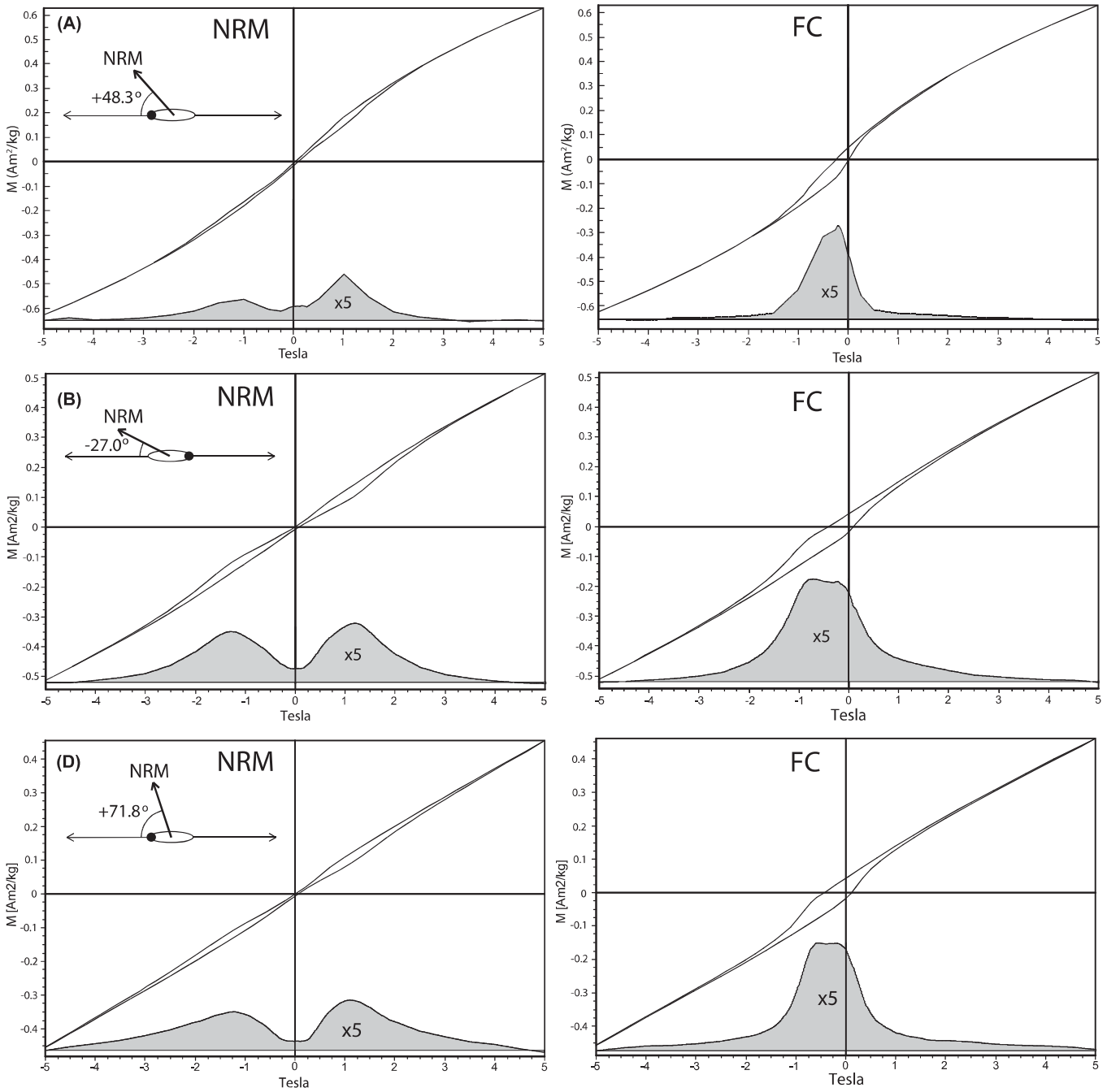

Figure 3(a). (A,B,D) Hysteresis loops for samples A, B and D, where the oriented NRM was placed toward the positive field direction of the MPMS. (**A-NRM**) Positive NRM placed 48.3° from negative direction of MPMS, equally favorable as 42.6° in Fig. 3F and 43.4° in Fig. S3I. Loop closures: –2.75, +2.63 T. Smaller loop separation at −1 T 0.017 Am^2 kg^{-1}, larger separation at +1 T 0.038 Am^2 kg^{-1}. Positive side greatly predominates. This is twin of Fig. 3G where the negative side predominates. This provides insight into the history of lamellar magnetization. Both A and G are from the same MOD-22-6 sample from material that undoubtedly cooled and exsolved at the same *T*, with a similar orientation to the Proterozoic magnetizing field. Thus, the main difference concerns negative (here) versus positive (G) placement in the MPMS. (**A-FC**) Predicted negative exchange bias. Loop closures: 1.88 and +1.88 T. Maximum loop separation at –0.19 T 0.076 Am^2 kg^{-1}. The different shapes of A-FC and G-FC could relate to the fact that, in order to achieve this negative exchange bias in FC, all the dominant negative lamellar remanence had to be overcome during field cooling in a positive field above T_N of ilmenite. By contrast, in G-FC, only the subordinate negative lamellar remanence had to be overcome. (**B-NRM**) Negative NRM placed 27° from negative direction of MPMS. Loop closures: –4.5 T and +4.35 T. Smaller loop separation at –1.30 T 0.034 Am^2 kg^{-1}, larger loop separation at +1.19 T 0.040 Am^2 kg^{-1}. Bimodal with positive side predominant. (**B-FC**) Predicted negative exchange bias. Loop closures: −4.25, +4.63 T. Maximum loop separation at –0.69 T 0.069 Am^2 kg^{-1}. (**D-NRM**) Positive NRM placed 71.8° from the negative direction of the MPMS like Fig. S3C. Apparent loop closures: –5 and +5 T. Smaller loop separation at –1.22 T 0.023 Am^2 kg^{-1}, larger loop separation at +1.10 T 0.030 Am^2 kg^{-1}. Bimodal with positive side predominant. (**D-FC**) Predicted negative exchange bias. Apparent loop closures: −5, +5 T. Maximum loop separation at −0.54 T 0.065 Am^2 kg^{-1}.

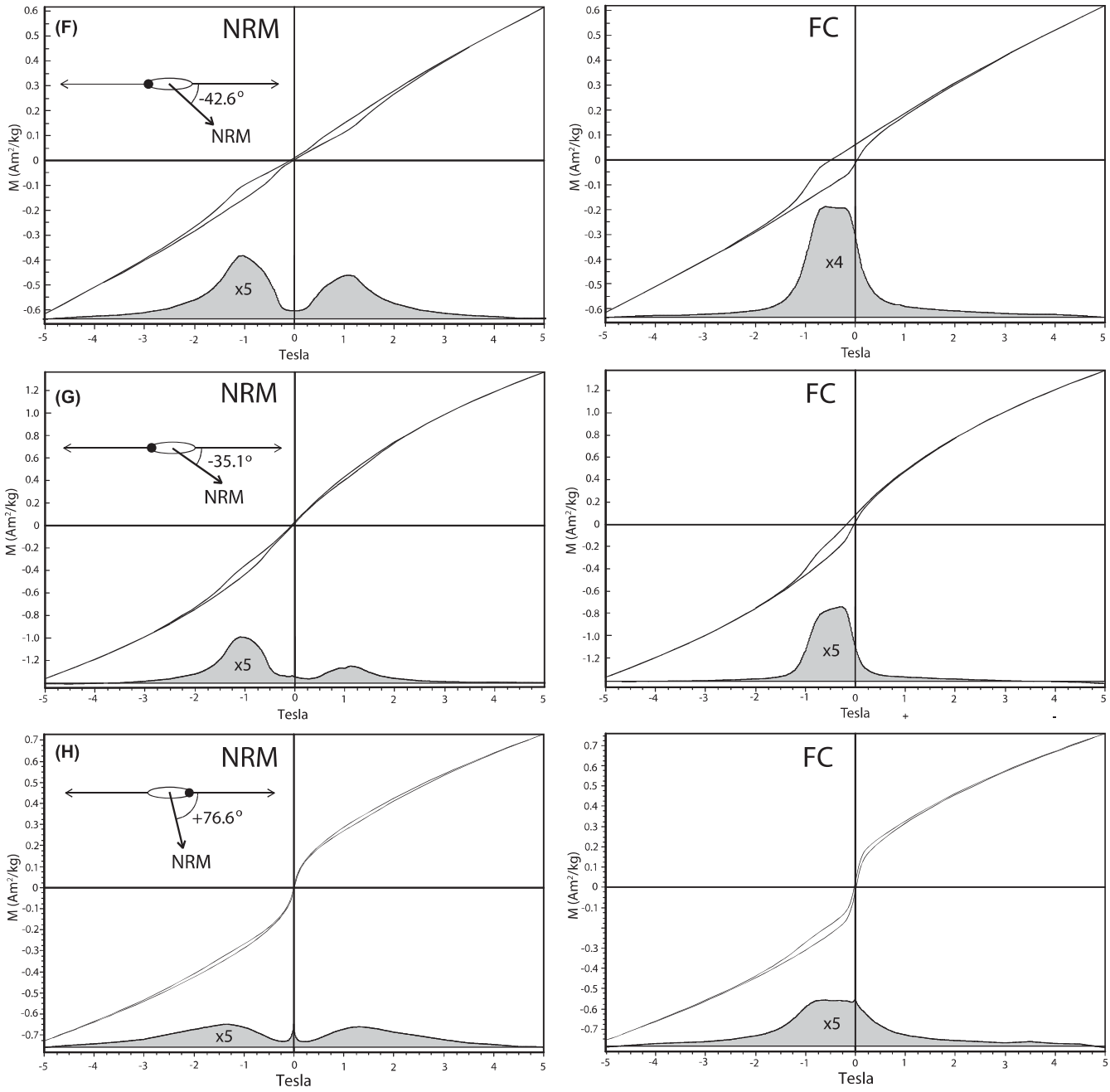

Figure 3(b). (F,G,H) Hysteresis loops for samples F, G, and H, where the oriented NRM was placed toward the negative field direction of the MPMS. (**F-NRM**) Negative NRM placed 42.6° from the positive direction of the MPMS. Loop closures: –3.8 and +3.55 T. Larger loop separation at –0.98 T 0.056 $Am^2\ kg^{-1}$, smaller loop separation at +1.08 T 0.038 $Am^2\ kg^{-1}$. Strikingly larger negative separation demonstrates that the dominant component of NRM, as placed positive in the MPMS, is stronger than the negative component. In all earlier 'unoriented' measurements, no NRM loop had a negative exchange bias. We were puzzled as to whether this was just by chance, or whether there was a deeper explanation. The first 'oriented' experiments in F, G and I provided examples of exactly that. (**F-FC**) Predicted negative exchange bias. Loop closures: −2.75, +3.0 T. Maximum loop separation at –0.57 T 0.081 $Am^2\ kg^{-1}$. (**G-NRM**) Negative NRM placed 35.1° from the positive direction of the MPMS, less favorable than 43.4 and 42.6° for Figs S3I and 3F. This sample has the strongest NRM (Table 2). Loop closures: –2.9 and +2.25 T. Larger loop separation at –1.04 T 0.082 $Am^2\ kg^{-1}$, smaller separation at +1.10 T 0.030 $Am^2\ kg^{-1}$. Bimodal loop with negative side greatly predominant. This is the most convincing example of negative exchange bias with positive placement of the NRM, yet more striking taking into account the smaller vertical scale compared to Fig. 3F. The more asymmetric bimodality here is consistent with an NRM neither parallel nor normal to the instrument field. (**G-FC**) Predicted negative exchange bias. Loop closures: −2.10, +2.13 T. Maximum loop separation at –0.28 T 0.133 $Am^2\ kg^{-1}$. (**H-NRM**) Positive NRM placed 76.6° from the positive direction of the MPMS. Loop closures: –4.9 and +4.7 T. Larger loop separation at –1.33 T 0.031 $Am^2\ kg^{-1}$, smaller separation at +1.31T 0.023 $Am^2\ kg^{-1}$. The loop is bimodal, with a very narrow center. Remarkable feature is steep central slope, both in this and in the FC loop, over the range from +0.2 T to –0.2 T. Represents a small fraction of magnetite, probably multi-domain, not coupled to titanohematite that was strongly magnetized below the Verwey transition. Also shown in the NRM loop by a very small central peak. Outside the central region the negative side predominates, thus another convincing example of a negative exchange bias. (**H-FC**) Predicted negative exchange bias. Loop closures: −4.25, +4.75 T. Maximum loop separation at –0.59 T 0.045 $Am^2\ kg^{-1}$.

Table 2. Comparisons of NRM intensity, (1) measured in the cryogenic magnetometer, (3) recalculated to intensity in the field direction of the MPMS, with (4) initial intensity measured in the MPMS at 300 K before field-free cooling.

Figure, sample, piece	(1) NRM Int.[a]	(2) Angle θ	(3) NRM cosθ[b]	(4) NRM measured[c]
Fig. 3A MOD22-6-C3	0.026813	−48.302	−0.0178	−0.01732
Fig. 3B MOD22-21b C4	0.006618	−27.029	−0.0059	−0.00533
Fig. 3C MOD22-6 C1	0.026064	−71.824	−0.0081	−0.00782
Fig. 3D MOD22-5-C5	0.018138	−71.827	−0.0057	−0.00628
Fig. 3E MOD22-8a-C5	0.014577	−11.397	−0.0142	−0.01560
Fig. 3F MOD22-5-C2	0.001921	+42.629	+0.0088	+0.00914
Fig. 3G MOD22-6-C2	0.045112	+35.120	+0.0369	+0.03390
Fig. 3H MOD22-21b C2	0.026726	+76.598	+0.0062[d]	+0.00040[d]
Fig. 3I MOD22-5-C1	0.006509	+43.404	+0.0047	+0.00428
Fig. 3J MOD22-8a C2	0.010058	+54.767	+0.0058	+0.00355

Notes. [a]NRM intensity in $Am^2\ kg^{-1}$ measured at 300 K in the cryogenic magnetometer.
[b]Calculated NRM intensity in $Am^2\ kg^{-1}$ in direction of capsule z axis (NRM_z).
[c]NRM intensity in $Am^2\ kg^{-1}$ measured at room T along the axis of the MPMS (also NRM_z)
[d]Only significant disagreement.

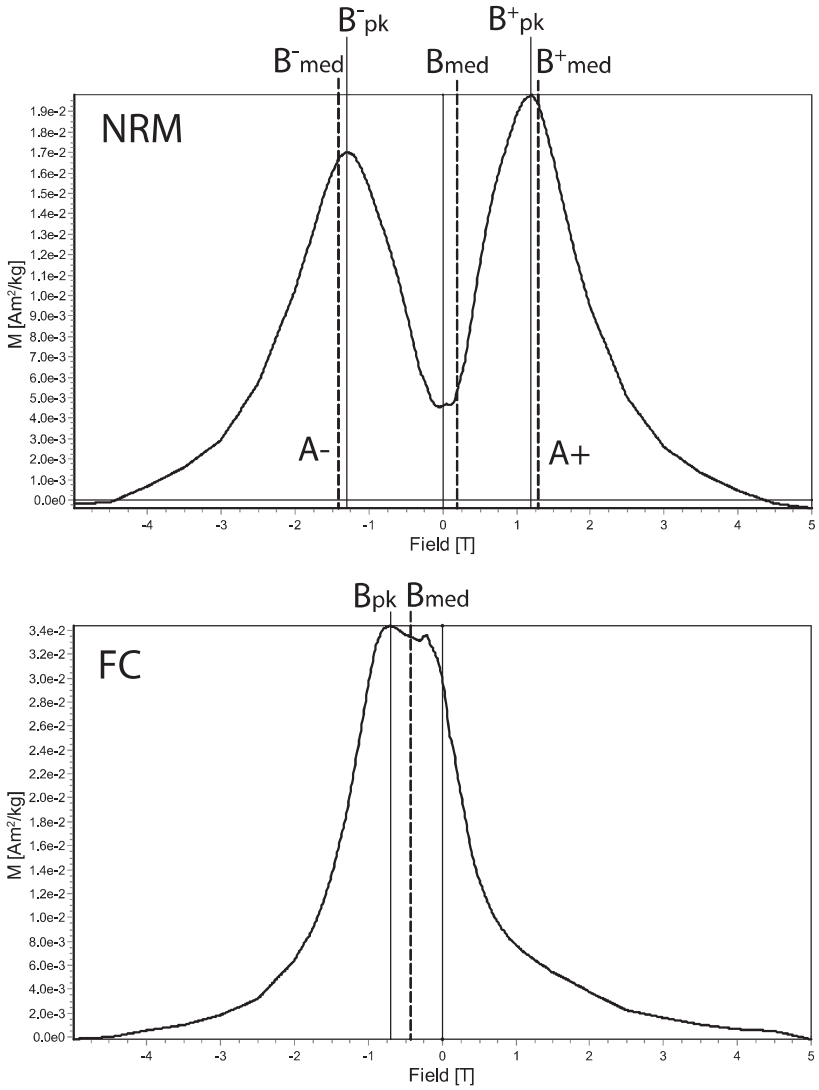

Figure 4. Examples of remanent hysterestic curves 'Mrh'(B) used in preparing shaded curves for samples A–J, for sample B in this specific example. These quantify the vertical half height of the loop separation at each field value: Mrh(B) = (M+(B) − M−(B))/2 (the full vertical height of the loop separation always exactly double this). For the NRM loops, the 'Mrh' curve is clearly bimodal, with three median fields (dashed vertical lines left to right) that, respectively, divide the negative-field area, the total area, and the positive-field area in half, and two modal fields (thin solid vertical lines). For the FC loops, the Mrh curve is generally unimodal, with a single median field (dashed vertical line) that divides the total area in half. The curve is rather flat-topped, and the peak and its associated modal field value (Bpk, thin solid vertical line) are not always well defined.

Table 3. Measured values in Tesla related to closure of low-*T* hysteresis loops. Samples are in two groups, first (3A–3E) those with NRM loops with a dominant positive opening, then (3F–3J) with a dominant negative opening. Loops marked in italics, summarized here, but graphics only available in electronic supplement.

Sample, piece, figure number, placement[a], loop type		(1) −Closure direct	(2) −Closure by 'Mrh'	(3) +Closure direct	(4) +Closure by 'Mrh'
MOD22-6, C 3	NRM	−2.75	−5.0	+2.63	+3.22,+4.08,+4.69
3A −48.3	FC	−1.88	−4.45,-3.71	+1.88	+4.88
MOD22-2-1b, C 4	NRM	−4.5	−4.7,-4.44	+4.35	+4.33
3B −27.0	FC	−4.25	−4.81,-4.54	+4.63	+4.88
MOD22-6, C 1	*NRM*	*∼−5*	*−4.94*	*∼+5*	*+4.83*
3C *−71.8*	*FC*	*∼−5*	*−4.94*	*∼+5*	*+4.88*
MOD22-5, C 5	NRM	∼−5	−5.0	∼+5	+4.73
3D −71.8	FC	∼−5	−4.96	∼+5	+5.23
MOD-22-8a, C 5	*NRM*	*−1.5*	*−4.49*	*+1.38*	*+2.36*
3E *−11.4*	*FC*	*−1*	*−4.96*	*+0.35*	*+1.85,+3.45, +4.52*
MOD22-5, C 2	NRM	−3.8	−4.9	+3.55	>5
3F +42.6	FC	−2.75	−4.88	+3.0	+4.96
MOD22-6, C 2	NRM	−2.9	−4.52,−3.83	+2.25	>5
3G +32.1	FC	−2.1	−4.38	+2.13	+3.77
MOD22−21b, C 2	NRM	−4.9	−4.96	+4.7	>+5
3H +76.6	FC	−4.25	−4.73	+4.75	+4.79
MOD22-5, C 1	*NRM*	*−3.3*	*−4.90*	*+3.25*	*+4.63*
3I *+43.4*	*FC*	*−1.85*	*−4.55*	*+2.05*	*+4.55*
MOD22-8a, C 2	*NRM*	*−2.125*	*−4.45*	*+1.4*	*+1.68,+1.74,+2.49*
3J *+54.8*	*FC*	*−1.35*	*−4.1i*	*+0.4*	*+0.73,+0.84,+0.96*

Note. [a]Acute angle that the NRM orientation makes with the MPMS in either a + or – direction. Negative angles are supplements to original positive obtuse angles listed in Table 1.

'squat': B, C, D and F. This is quantified by measuring the distances between M(+5T) and Mr_{AV}, between M(−5T) and Mr_{AV}, or taking the absolute averages between these results (Table 5, columns 6, 7, 8). In this, four of the five 'tall' loops show averages 0.729 to 3.66, except A, which is 0.627. Two of the four 'squat' loops show averages 0.455 and 0.512, but two, C and F, show averages 0.623 and 0.618, that essentially overlap with the borderline case A in the 'tall' group. Thus it appears that these averages work well except for loops with intermediate character.

Another key feature is that the values for Mr– and Mr+ and their average, Mr_{AV}, are systematically offset from the middle position between the –5 T and +5 T intercepts. For the NRM loops with negative placement of NRM_Z (3A–3E), the Mr_{AV} values are systematically offset in a negative direction. This is shown by the larger value of the difference M(+5T) – Mr_{AV} compared to the difference M(–5 T) – Mr_{AV} (Table 5, columns 6, 7). For the NRM loops with positive placement of NRM_z (3F–3J), and for the FC loops, the Mr_{AV} values are systematically offset in a positive direction. This is shown by the larger value of the difference M(−5T) – Mr_{AV} compared to the difference M(+5T) – Mr_{AV} (Table 5, columns 7,6). There is complete consistency in these numerical relationships for all ten samples and 20 loops.

We know that the positive and negative effects described above result from AF coupling at low *T* between the lamellar NRM and the strong low-*T* remanence of ilmenite. In a phase with very high coercivity that is not fully saturated at high fields, there would be a shift away from symmetry of the high field +5 T and –5 T intercepts. Such an effect can be described as a 'remanence shift' of the hysteresis loop, which would cause both high-field intercepts to shift together either upward or downward. From negative or positive placement of NRM_Z, we can be sure that the coupled moment of the ilmenite is positive in the case of negative placement (3A–3E) and negative in the case of positive placement (3F–3J). Therefore, the intercepts would be shifted upward for 3A–3E and downward for 3F–3J. Comparisons of these intercepts, M(–5T) and M(+5T), shows very small differences in the values (Table 5 columns 1,2), and no systematic relationship according to the ideal predictions just given. In effect, these data indicate that there is no significant remanence shift in these samples, in spite of the obvious fact that magnetic properties of ilmenite control the magnetic exchange bias.

A tentative conclusion is that although magnetic coupling with magnetized ilmenite causes asymmetric behavior of the lamellar magnetism in the region between –5 T and +5 T, the actual collective remanent moment of the ilmenite itself compared to the lamellar magnetism of the host, is very weak. Thus, there is no remanence shift, while at the same time coupling on interfaces of magnetized ilmenite has a large effect on the interior of the loops, both the NRM loops and the subsequent FC loops. These relationships provide key insights for creating physical-magnetic models that are discussed in Paper III of this series.

Another aspect of the hysteresis measurements provides a powerful additional argument about the 'hardness' of ilmenite remanence. Once the ilmenite magnetization is established by AF coupling to the lamellar magnetism that is in effect when the sample passes through T_N of the ilmenite, it does not change its main orientation in fields of 5 T. In the five NRM loops where NRM_Z was inserted positively, a predominant negative ilmenite magnetization was created, and this was retained even in fields of +5 T, as shown by the positive values of Mr_{AV} when that field was removed. In the 10 FC

Table 4. Low-*T* hysteresis loop (1) maximum separation (peak) positions in T, (2) maximum separation (peak) heights in $Am^2\ kg^{-1}$, and (3) separation (peak) areas in $J\ kg^{-1}$. Bold indicates larger of two equivalent absolute values for negative and positive openings of NRM loops.

Sample, piece placement, loop type[a]		(1) Max. separation (peak) position[b] B-pk	B+pk	(2) Max. separation (peak) height[b] $Am^2\ kg^{-1}$ (%)		(3) Separation (peak) area[c] $J\ kg^{-1}$ (%)	
MOD22-6,C3	NRM	−1.000	+1.000	0.0172(31.2)	**0.0379(68.8)**	0.016(42.1)	**0.022(57.9)**
3A −48.3[d]	FC	−0.188		0.0760		0.045	
MOD22-2-1b,C4	NRM	**−1.299**	+1.188	0.0341(46.2)	**0.0397(53.8)**	0.032(48.5)	**0.034(51.5)**
3B −27.0[d]	FC	−0.694		0.0688		0.078	
MOD22-6,C1	*NRM*	***−1.186***	*+1.083*	*0.0237(42.5)*	***0.0321(57.5)***	*0.029(46.8)*	***0.033(53.2)***
3C *−71.8*[d]	*FC*	*−0.296*		*0.0805*		*0.072*	
MOD22−5,C5	NRM	**−1.217**	+1.104	0.0229(43.4)	**0.0299(53.6)**	0.027(47.4)	**0.030(52.6)**
3D −71.8[d]	FC	−0.541		0.0646		0.066	
MOD-22-8a,C5	*NRM*	***−0.500***	*+0.479*	*0.0279(40.7)*	***0.0406(59.3)***	*0.0208(49.5)*	***0.021(50.5)***
3E *−11.4*[d]	*FC*	*−0.156*		*0.1388*		*0.046*	
MOD22-5, C2	NRM	−0.980	**+1.083**	**0.0555(59.2)**	0.0382(40.8)	**0.040(57.1)**	0.030(42.9)
3F +42.6[d]	FC	−0.571		0.0814		0.079	
MOD22-6,C2	NRM	−1.041	**+1.104**	**0.0819(73.1)**	0.0301(26.9)	**0.048(68.6)**	0.022(31.4)
3G +32.1[d]	FC	−0.281		0.1333		0.077	
MOD22-21b,C2	NRM	**−1.330**	+1.313	**0.0308(56.8)**	0.0234(43.2)	**0.025(53.2)**	0.022(46.8)
3H +76.6[d]	FC	−0.592		0.0453		0.058	
MOD22-5,C1	*NRM*	*−1.093*	***+1.094***	***0.0378(57.3)***	*0.0282(42.7)*	***0.040(55.5)***	*0.032(44.4)*
3I *+43.4*[d]	*FC*	*−0.104*		*0.1113*		*0.075*	
MOD22-8a,C2	*NRM*	*−0.583*	***+0.585***	***0.0230(55.2)***	*0.0187(44.8)*	***0.017(63.0)***	*0.010(37.0)*
3J *+54.8*[d]	*FC*	*−0.146*		*0.0892*		*0.029*	

[a]Samples are in two groups, first those with NRM loops with a dominant positive opening (3A–3E), then with dominant negative openings (3F–3J). Loops marked in italics, summarized here, only available in electronic supplement.
[b]Position in T of the maximum vertical (peak) separation between curves measured from an 'Mrh' plot (see Fig. 4). For the bi-modal NRM loops with two peaks, the peak with the larger shift is marked in bold.
[c]Vertical separation (peak) height in $Am^2\ kg^{-1}$. This is double the value taken from 'Mrh' plots (Fig. 4). For the bi-modal NRM loops the opening with the higher vertical separation is marked in bold (%) indicates the percentage of the height of this peak compared to the total of the two peaks.
[d]Calculated area separation of hysteresis loop in $J\ kg^{-1}$, converted from vertical scale in $Am^2\ kg^{-1}$ and horizontal scale in T. For the bi-modal NRM loops, the areas are divided at zero field and the value for the larger area is marked in bold. (%) Indicates the percentage of the area of this peak compared to the total area of the two peaks. Acute angle that the NRM orientation makes with the MPMS in either a + or – direction. Negative angles are supplements to original positive obtuse angles listed in Table 1.

loops the argument is stronger. When the samples with a strong lamellar magnetism induced in a +5 T field are cooled below T_N of ilmenite, AF coupling with the hematite host causes the ilmenite to magnetize negatively in spite of the strong positive field and at 5 K that orientation stays essentially fixed regardless of subsequent application of 5 T fields. These results are against a hypothesis that movement of domain walls in the hematite hosts can be the main cause of these asymmetric hysteresis loops, but we think such walls are still potentially important in details of the hysteresis effects.

6.5 Quantifying magnetic exchange bias

In an exchange-biased hysteresis loop, the center of the loop is not in the zero-field position (center of the diagram), but is shifted to a positive or negative location. There are three common methods to quantify the hysteresis shift.

The first method is to quantify the area between the upper and lower limbs and then to find the median field B_{med} of that area (i.e., the field value that divides the area in half). The area is the product of magnetization (in $Am^2\ kg^{-1}$) and field (in T) and thus has units of $J\ kg^{-1}$, giving B_{med} as illustrated in Fig. 4. Where a hysteresis loop has two maximum (peak) separations, one in the positive field and one in the negative, the loop areas can be divided into two parts, separated by the location of narrowest separation between. Here, we found it difficult to locate this narrowest separation precisely and decided to divide the bimodal loop areas at the position of zero field. The two areas A^+ and A^- each have an associated median field, B^+_{med} and B^-_{med}, respectively. Fig. 4 shows examples of this for Fig. 3B and the same terminology is used to describe the lists in Table 6.

The second method is to subtract the lower limb from the upper limb to obtain the maximum separation (peak) height between them and locate this peak in T. This can be done using versions of Fig. 3 directly, but is more effectively accomplished using Mrh yielding B-pk and B+pk for NRM loops and B-pk for FC loops as illustrated in Fig. 4 and listed in Table 6. The first five data sets are from samples where the NRM was placed negatively in the MPMS. The second five data sets are from samples where the NRM was placed positively. The FC loops in all ten figures showed negative unimodal exchange bias consistent with cooling in a +5 T field.

The third method is to measure the coercivity in T of the upper limb and lower limb at the location of widest horizontal separation between the limbs. This is usually at the location of the largest vertical separation. The hysteresis shift, formally H_E, is then the average Tesla value between the upper and lower limb positions. In most examples this will be very close to Bpk values presented here and we did not pursue this third method.

Table 5. Values of magnetization at –5 and + 5 T, values of remanence from hysteresis loops at 5 K, and combinations that relate to shape of loops in Fig. 3. Where two values are compared (see text), larger absolute value is in bold.

Figure, placement, loop type[a]		(1) M(–5 T)[b] ($Am^2\ kg^{-1}$)	(2) M(+5 T)[c] ($Am^2\ kg^{-1}$)	(3) Mr+[d] ($Am^2\ kg^{-1}$)	(4) Mr–[e] ($Am^2\ kg^{-1}$)	(5) MrAv[f] ($Am^2\ kg^{-1}$)	(6) M(+5T) –MrAv[g] ($Am^2\ kg^{-1}$)	(7) M(-5T) –MrAv[h] ($Am^2\ kg^{-1}$)	(8) Absol. MrAv[i] ($Am^2\ kg^{-1}$)
3A −48.3[j]	NRM	−0.6268	**0.6275**	−0.00588	**−0.01719**	−0.01153	**0.6390**	−0.6153	0.6272 **I**
	FC	−0.6249	**0.6289**	**+0.04739**	−0.00528	+0.02106	0.6078	**−0.6460**	0.6269 **I**
3B −27.0[j]	NRM	**−0.5125**	0.5122	+0.00143	**−0.00775**	−0.00316	**0.5154**	−0.5093	0.5124 **S**
	FC	−0.5119	**0.5151**	**+0.04246**	0.01760	+0.01243	0.5027	**−0.5243**	0.5135 **S**
3C −71.8[j]	*NRM*	*−0.6223*	***0.6229***	*−0.00101*	***−0.01087***	*−0.00594*	***0.6288***	*−0.6164*	*0.6226* ***I***
	FC	*−0.6626*	***0.6695***	***+0.05137***	*−0.01522*	*+0.01808*	*0.6514*	***−0.6807***	*0.4591* ***S***
3D −71.8[j]	NRM	**−0.4552**	0.4548	−0.00093	**−0.00630**	−0.00361	**0.4584**	−0.4516	0.4550 **S**
	FC	−0.4571	**0.4610**	**+0.04210**	−0.01887	+0.01162	0.4494	**−0.4687**	0.4591 **S**
3E −11.4[j]	*NRM*	***−2.6108***	*2.6105*	*+0.00653*	***−0.02523***	*−0.00935*	**2.6199**	−2.6015	2.6107 **T**
	FC	***−2.6134***	*2.6133*	***+0.07792***	*−0.01109*	*+0.03342*	2.5799	**−2.6468**	2.6134 **T**
3F +42.6[k]	NRM	−0.6176	**0.6177**	**+0.01027**	+0.00301	+0.00664	0.6111	**−0.6242**	0.6177 **I**
	FC	−0.6150	**0.6202**	**+0.06043**	−0.01532	+0.02256	0.5976	**−0.6376**	0.6176 **I**
3G +32.1[k]	NRM	−1.3658	**1.3660**	**+0.02991**	+0.01895	+0.02443	1.3416	**−1.3902**	1.3659 **T**
	FC	−1.3739	**1.3774**	**+0.08238**	+0.01932	+0.05085	1.3266	**−1.4248**	1.3757 **T**
3H +76.6[k]	NRM	**−0.7298**	0.7286	**+0.00855**	−0.00809	+0.00023	0.7284	**−0.7300**	0.7292 **T**
	FC	−0.7562	**0.7574**	**+0.03321**	−0.01231	+0.01045	0.7470	**−0.7667**	0.7568 **T**
3I + 43.4[k]	*NRM*	***−1.1363***	*1.1343*	***+0.01750***	*−0.01048*	*+0.00351*	1.1308	**−1.1398**	1.1353 **T**
	FC	*−1.3751*	***1.3766***	***+0.06211***	*−0.03697*	*+0.01257*	1.3640	**−1.3877**	1.3759 **T**
3J +54.8[k]	*NRM*	***−3.6673***	*3.6617*	***+0.01086***	*−0.00713*	*+0.00186*	3.6598	**−3.6692**	3.6645 **T**
	FC	***−3.6551***	*3.6495*	***+0.05035***	*−0.01276*	*+0.01880*	3.6307	**−3.6739**	3.6523 **T**

Notes. [a]Loops are listed according to NRM loops, 3A–3E with negative sample placement and dominant positive opening, 3F–3J with positive sample placement and dominant negative opening. Italics indicate loops summarized here but only available in electronic supplement.
[b]Value of total magnetization recorded in a field of –5 T.
[c]Value of total magnetization recorded in a field of +5 T.
[d]Value of remanent magnetization recorded in zero field on upper limb of loop on return from +5 T. Shows consistent positive and larger absolute value for the bi-modal NRM loops 3F–3J for samples placed positively, for all of which the negative peak predominates.
[e]Value of remanent magnetization recorded in zero field on lower limb of loop on return from –5 T. Shows consistent negative and larger absolute value for the bi-modal NRM loops 3A–3E for samples placed negatively, for all of which the positive peak predominates.
[f]Calculated average (midpoint) in zero field between remanence values recorded on upper and lower limbs of hysteresis loop.
[g]Value in $Am^2\ kg^{-1}$ of total magnetization recorded in a field of +5 T minus Mr Av (midpoint).
[h]Value in $Am^2\ kg^{-1}$ of total magnetization recorded in a field of –5 T minus Mr Av (midpoint).
[i]Average of absolute values M(+5 T) minus Mr Av and M(–5 T) minus Mr Av. Letters indicate loops classified as squat (**S**), tall (**T**) or intermediate (**I**).
[j]Sample was placed parallel to the negative field direction of the MPMS and the 'NRM loop' gave a predominant positive bi-modal exchange bias.
[k]Sample was placed parallel to the positive field direction of the MPMS and the 'NRM loop' gave a predominant negative bi-modal exchange bias.

In Table 6, column 1, the total areas of NRM loops and corresponding FC loops are compared. The areas of the FC loops are on average 20 per cent larger than the corresponding NRM loops. The shapes of the NRM loops are mainly controlled by ilmenite magnetization, which was responding to a lamellar NRM, created in a weak Earth field, and here cooled to below T_N of ilmenite. By contrast the FC loops are mainly controlled by ilmenite magnetization created when a lamellar magnetism, approximately saturated in a +5 T at 300 K, was cooled below T_N of ilmenite. What is perhaps surprising is that the application of the strong field before field cooling did not result in a significantly larger lamellar magnetism that would be reflected in a very much larger unimodal hysteresis loop. This may be related to what has been described as the remarkable efficiency of natural lamellar magnetism (McCammon *et al.* 2009).

Table 6, column 2, shows the median fields B_{med} for the NRM and FC loops. The median fields for the FC loops are negative, consistent with the fact that the ilmenite magnetizations were produced by strong AF coupling to lamellar magnetism created in a +5 T field. The median fields of the first five NRM loops, 3A–3E, are consistently positive in agreement with negative placement of the NRM. The median fields of the last five NRM loops, 3F–3J, are consistently negative in agreement with positive placement of the NRM. Comparisons of the absolute values of the median fields of the NRM and FC loops show inconsistency. NRM values predominate in 3A, 3C, 3D, 3F, 3G, 3H, 3J and FC values in 3B, 3E and 3I.

Table 6, columns 3,4,5,6, compare the results where the negative and positive portions of the bimodal NRM loop were measured separately (i.e. the peak and median fields of A^+ and A^-). Columns 3,4 also list equivalent values for the negative unimodal FC loops.

For the first five NRM loops, 3A–3E, the results are very consistent. For the negative separation peaks, the negative median field values are consistently larger than the maximum separation peak height values. For the positive separation peaks, the positive median field values are consistently larger than the maximum separation peak height values. This is a loop shape where the areas are

Table 6. Comparisons of two methods (see Fig. 4) to describe the degree of magnetic exchange bias: by the median field in T for the calculated loop separation (peak) area (columns 3 and 6), and by position in T of the maximum loop separation (peak) (columns 4 and 5). All loops can be characterized by total loop area and median field (columns 1 and 2). FC loops show only one dominant negative opening and graphic peak. NRM loops show two openings, two graphic peaks, and one median field for each of the two peaks. Where two or more values are compared (see text), larger (largest) absolute value is in bold. Where four values are compared, second largest value is underlined.

Figure number, placement[a], loop type		(1) Total Loop Area (J kg^{-1})[b]	(2) Median field Bmed[c]	(3) Negative Med.Field B-med[d]	(4) Negative Peak B-pk[e]	(5) Positive Peak B+pk[f]	(6) Positive Med.Field B+med[g]
3A −48.3	NRM	0.0380	+0.510	**−1.281**	−1.000	+1.000	+1.052
	FC	**0.0456**	−0.344	**−0.344**	−0.188		
3B −27.0	NRM	0.0663	+0.199	**−1.406**	−1.299	+1.188	+1.299
	FC	**0.0779**	−0.426	−0.426	**−0.694**		
3C −71.8	*NRM*	*0.0615*	*+0.350*	***−1.643***	*−1.186*	*+1.083*	*+1.471*
	FC	***0.0719***	*−0.286*	***−0.286***	*−0.296*		
3D −71.8	NRM	0.0564	+0.415	**−1.654**	−1.217	+1.104	+1.482
	FC	**0.0660**	−0.307	−0.307	**−0.541**		
3E −11.4	*NRM*	*0.0420*	*+0.010*	***−0.760***	*−0.500*	*+0.479*	*+0.573*
	FC	***0.0459***	*−0.260*	***−0.260***	*−0.156*		
3F +42.6	NRM	0.0705	−0.555	−1.169	−0.980	+1.083	**+1.223**
	FC	**0.0792**	−0.393	−0.393	**−0.571**		
3G +32.1	NRM	0.0694	−0.835	−1.105	−1.041	+1.104	**+1.212**
	FC	**0.0771**	−0.436	**−0.436**	−0.281		
3H +76.6	NRM	0.0471	−0.404	**−1.676**	−1.330	+1.313	+1.643
	FC	**0.0576**	−0.393	−0.393	−0.592		
3I +43.4	*NRM*	*0.0721*	*−0.296*	***−1.234***	*−1.093*	*+1.094*	*+1.191*
	FC	***0.0753***	*−0.307*	***−0.307***	*−0.104*		
3J +54.8	*NRM*	***0.0271***	*−0.350*	***−0.803***	*−0.583*	*+0.585*	*+0.566*
	FC	*0.0288*	*−0.243*	***−0.243***	*−0.146*		

Notes. Loops are listed according to NRM loops, 3A–3E with negative sample placement and dominant positive opening, 3F–3J with positive sample placement and dominant negative opening. Italics indicate loops only available in electronic supplement.
[a]Angle of the NRM with respect to positive or negative field direction in the single-axis MPMS.
[b]Calculated area of hysteresis loop in J kg^{-1}, converted from vertical scale in Am^2 kg^{-1} and horizontal scale in T.
[c]Value in T at the median of calculated loop area (Bmed), where NRM loop was not divided in two.
[d]Value in T at the median of the calculated area of the negative part of the NRM loop (B-med) or the FC loop (repeats column 2).
[e]Value in T at maximum separation (peak) height of the negative part of the NRM loop (B-pk) or the FC loop.
[f]Value in T at maximum separation (peak) height of the positive part (B+pk) of the NRM loop.
[g]Value in T at the median of the calculated area of the positive part of the NRM loop (B+med).

skewed toward higher values in both negative and positive directions. In Fig. 2 it is easy to see that for a negative peak (on the left) it requires a stronger negative field to approach saturation in the exchange-biased state and only a weak positive field to return to the full equilibrium state. Conversely for a positive peak (on the right) it requires a stronger positive field to approach saturation in the exchange-biased state and only a weak negative field to return to the full equilibrium state. Here, the negative loop with the smaller area shows a larger absolute shift in median field than the positive loop with the larger area. Three of the negative separation peaks in Table 6(B, C, D) {note that C is not shown in Fig. 3} have shifts at –1.41, –1.64 and –1.65 T, and two of the positive separation peaks (C, D) have shifts at +1.46 and +1.48 T, and show larger absolute shifts than were measured in the same way on a MOD2 sample at –1.34 T (McEnroe *et al.* 2007a; Fabian *et al.* 2008).

For the second set of five NRM loops, 3F–3J, the results are nearly as consistent. For the negative separation peaks, the negative median field values are consistently larger than the maximum separation peak height values. For the positive separation peaks, the positive median field values are consistently larger than the maximum separation peak values (excluding 3J). Again, this is a loop shape where the areas are skewed toward higher values in both negative and positive directions, and the explanation given above with reference to Fig. 2 should apply here. Of these five loops, 3F, 3G, show a larger absolute shift in median field for the positive loop separation with the smaller area than for the negative loop separation with the larger area, consistent with the situation for 3A–3E. However, for 3H–3J, the median field shift is slightly larger for the negative loop with the larger area. Note that 3H is complicated by presence of magnetite. For 3H, both the negative loop shift –1.68 T and the positive loop shift at +1.64 T are larger than the absolute shift of –1.34 T measured on a MOD2 sample. The negative FC loop Tesla values for median field and maximum separation peak show no consistent relationship.

6.6 Relationships between NRM_Z and several hysteresis properties

Fig. 5 shows the relationships between Mr+, the loop intercept of the upper limb at zero field; Mr–, the loop intercept on the lower limb;

Table 7. Measurements at 5 K of the average remanence at zero field (MrAv) compared to the component of the NRM (300 K) parallel to the MPMS field direction (NRM_Z). Results are compared in Fig. 5.

Sample, piece placement, type		Mr+ Upper limb[a]	Mr– Lower limb[b]	Mr average[c]	NRM Parallel to axis[d]	Correlation MrAv/NRM_Z[e]
MOD22-6, C 3	NRM	−0.00588	−0.01719	−0.01153	−0.01730	0.667
3A −48.3[f]	FC	0.04739	−0.00528	0.02105		−1.217
MOD22-2-1b, C 4	NRM	0.00143	−0.00775	−0.00316	−0.00533	0.592
3B −27.0[f]	FC	0.04246	−0.01760	0.01243		−2.332
MOD22-6, C 1	*NRM*	*−0.00101*	*−0.01087*	*−0.00594*	*−0.00782*	*0.760*
3C *−71.8*[f]	*FC*	*0.05137*	*−0.01522*	*0.01807*		*−2.311*
MOD22-5, C 5	NRM	−0.00093	−0.00630	−0.00361	−0.00628	0.576
3D −71.8[f]	FC	0.04210	−0.01887	0.01162		−1.850
MOD-22-8a, C 5	*NRM*	*0.00653*	*−0.02523*	*−0.00935*	*−0.01560*	*0.599*
3E *−11.4*[f]	*FC*	*0.07792*	*−0.01109*	*0.03341*		*−2.142*
MOD22-5, C 2	NRM	0.01027	0.00301	0.00664	0.00914	0.726
3F +42.6[f]	FC	0.06043	−0.01532	0.02256		2.468
MOD22-6, C 2	NRM	0.02991	0.01895	0.02443	0.03390	0.721
3G +32.1[f]	FC	0.08238	0.01932	0.05085		1.500
MOD22-21b, C 2	NRM	0.00855	−0.00809	0.00023	0.000399	0.578
3H +76.6[f]	FC	0.03321	−0.01231	0.01045		26.189
MOD22-5, C 1	*NRM*	*0.01750*	*−0.01048*	*0.00351*	*0.00428*	*0.820*
3I *+43.4*[f]	*FC*	*0.06211*	*−0.03697*	*0.01257*		*2.936*
MOD22-8a, C 2	*NRM*	*0.01086*	*−0.00713*	*0.00186*	*0.00355*	*0.525*
3J *+54.8*[f]	*FC*	*0.05035*	*−0.01276*	*0.01879*		*5.294*

Notes. Samples are in two groups, first those with NRM loops with a dominant positive opening (3A–3E), then with dominant negative opening (3F–3J). Loops marked in italics, summarized here, are only available in electronic supplement.
[a]Intercept of upper hysteresis limb on zero field axis at 5 K.
[b]Intercept of lower hysteresis limb on zero field axis at 5 K.
[c]Average of intercepts on zero field axis at 5 K.
[d]Component of the 300 K NRM measured parallel to the capsule axis (NRM_Z) in the cryogenic magnetometer prior to placing in the MPMS.
[e]Ratio of the average Mr (MrAv) to the value of NRM parallel to the MPMS axis (NRM_Z). Gives a preliminary view of correlations between these values, more strikingly shown in Fig. 5. Trend line $y = 0.6935x + 0.0004$, $R^2 = 0.9961$.
[f]Acute angle that the NRM orientation makes with the MPMS in either a + or – direction. Negative angles are supplements to original positive obtuse angles listed in Table 1.

and Mr_{AV}, the average of Mr+ and Mr–; versus NRM_Z. Fig. 5NRM shows the values from NRM loops where positive and negative placements of NRM_Z give different results for Mr+, Mr_{AV} and Mr–. Fig. 5FC shows the values from FC loops where positive and negative placements of NRM_Z are not relevant because of cooling in a strong positive field. Here Mr+, Mr_{AV} and Mr– are plotted against the absolute values of NRM_Z.

Fig. 5 shows that there is no constant relationship between the separation of zero field intercepts of the upper limb (Mr+) and of the lower limb (Mr–) and NRM_Z. This separation in the NRM loops is more closely related to the 'tallness' or 'squatness' of the loops, where the 'tall' loops appear to show a much higher ratio of induced to remanent magnetization. Contrary to visual perceptions from Fig. 3, it is the loops with seemingly 'skinny' loop separations, E, I and J (electronic supplement) that show the largest separations at zero field, whereas the loops that one perceives to have higher loop separations at zero field, B, C, D and F, in fact have smaller loop separations, misperceived as larger because Fig. 3 shows them with a larger vertical scale. For discussion of 'tall', 'intermediate' and squat' loops, refer back to Section 6.4 and Table 5.

Because of poor correlations between the separations between Mr+ and Mr– versus NRM_Z, as in Fig. 5, the correlations between Mr+ versus NRM_Z and Mr– versus NRM_Z in the same figure are poor, as shown by the corresponding trend lines and coefficients. It is then surprising for the NRM loops, to find a very strong correlation in Fig. 5NRM of Mr_{AV} versus NRM_Z, where both Mr_{AV} and NRM_Z can be either positive or negative (center of Fig. 5NRM). The trend line is $y = 0.6935x + 0.0004$, $R^2 = 0.9961$, passing near the origin. The similar plot for FC loops (Fig. 5FC) using the absolute value of NRM_Z shows a weaker trend line $y = 1.1905x + 0.0088$, $R^2 = 0.8699$ passing well above the origin, consistent with the fact that the +5 T field cooling before the FC loops makes all values more positive.

The negative loop separation peak area minus the positive loop separation peak area plotted against NRM_Z gives a trend line $y = 0.6334x + 0.0039$, $R^2 = 0.9251$. The negative loop separation peak height minus the positive loop separation peak height plotted against NRM_Z gives a trend line $y = 1.3811x + 0.0037$, $R^2 = 0.9821$. A feature of these comparisons already noted in Table 4 is how close most of the positive and negative loops loop separations are to being equal in area or height. The one exception to this is sample G, which one can see is unusual in several ways.

The strong correlation in Fig. 5NRM shows that the NRM_Z measured at room T in the cryogenic magnetometer is an excellent predictor of the average remanence, Mr_{AV}, measured in zero field at 5 K. Mr_{AV} is related to the amount of AF coupling between the original lamellar magnetism and the ilmenite magnetism which

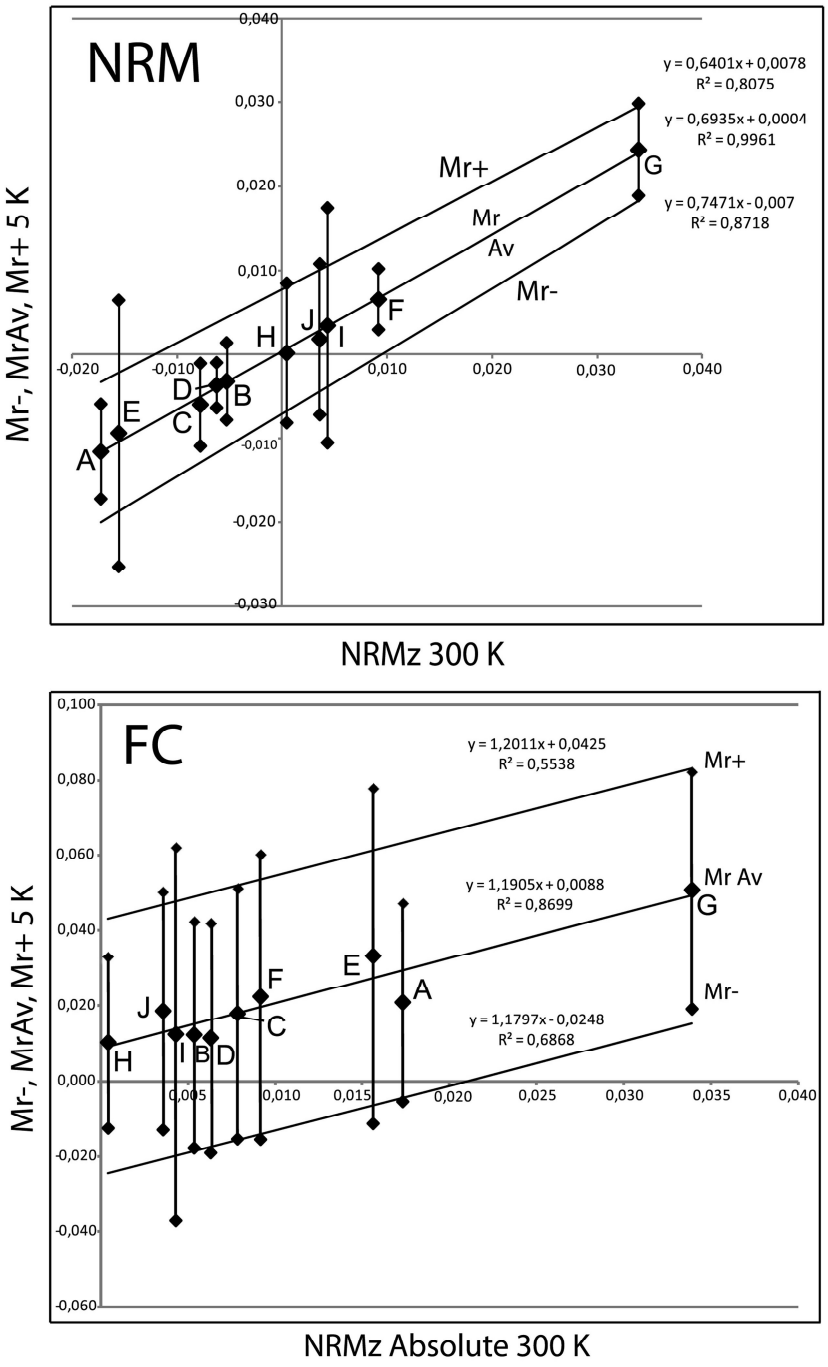

Figure 5. Plots of Mr+, MrAv (average) and Mr− measured in zero field at 5 K versus NRM_Z (component of natural remanent magnetization at room *T* parallel to the field direction of the MPMS). (NRM) Results from NRM loops where NRM_Z and MrAv can be either positive or negative. (FC) Results from FC loops where sample was cooled in +5 T field overriding the NRM and resulting only in positive values of MrAv. Here the Mr values are plotted against the absolute value of NRM.

only came into effect at ∼57 K, and where the coupling hardened substantially between 57 and 5 K. The proportionality coefficient of 0.69 (ratios 0.576–0.820) suggests something about the efficiency of that coupling, that is the amount of coupling or the way it is expressed, is about 69 per cent of the value of NRM_Z. This correlation is complimented by additional correlations obtained from the results of cooling and warming experiments discussed in Section 7.

We have considered this correlation in two ways: (1) as a function of angular relationships in any sample between the NRM_Z orientation and the orientation of the ilmenite magnetization. (2) As a function of a growth model for ilmenite lamellae in a hematite host. The truth likely includes both of these relationships. Because these relationships are quite complex and involve physical relationships of model lamellae, populations of lamellae within crystals, and populations of crystals in rock with or without lattice-preferred orientation, we postpone further detailed discussion to Paper III. The particular growth model would produce an ilmenite lamella with a net ilmenite magnetic moment of zero, in line with the discussion in Section 6.4, where it was shown that the loops show no ‘remanence

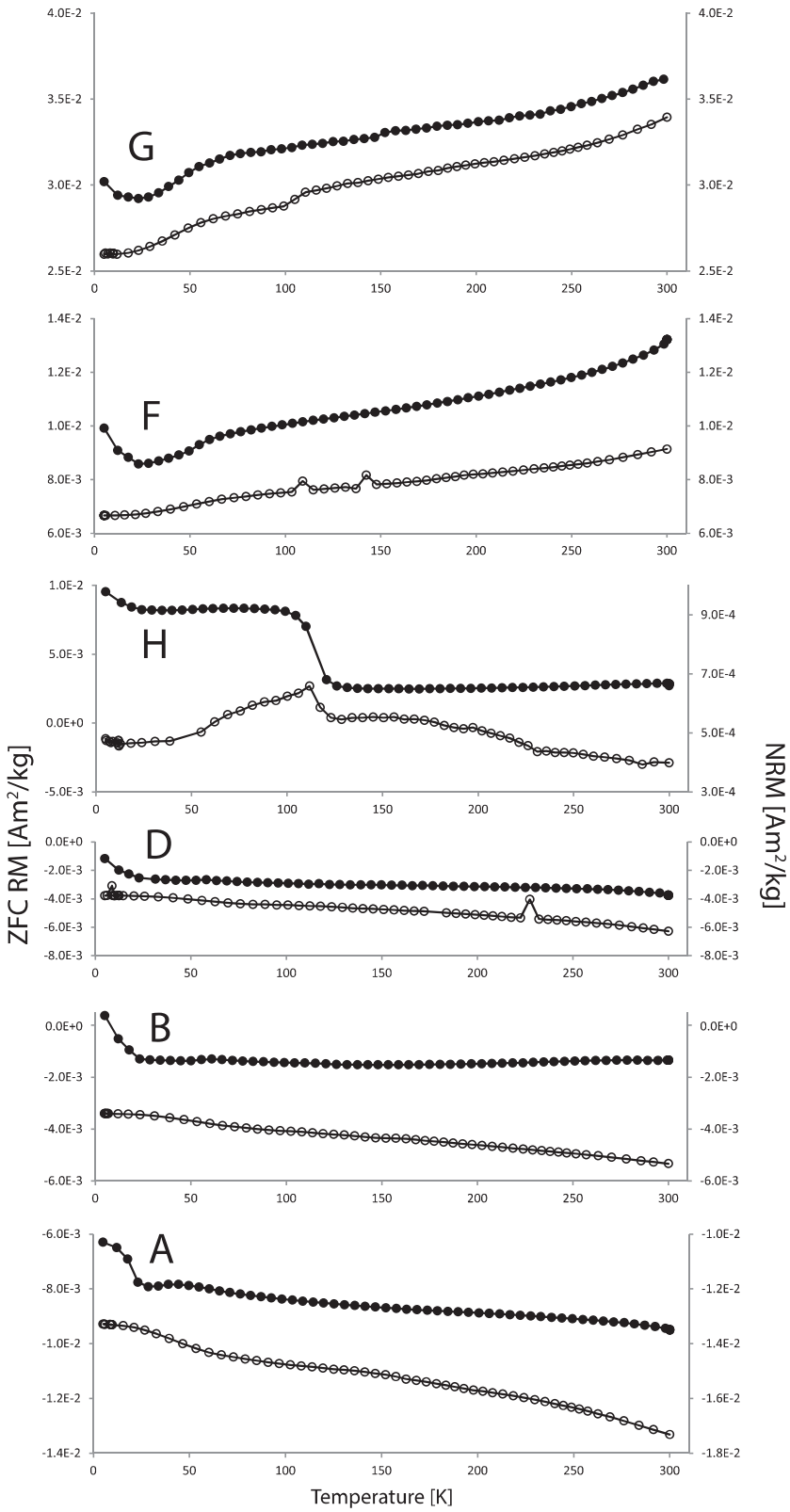

Figure 6. Plots showing the magnetization in the field direction of the MPMS during FF cooling 300 to 5 K before NRM hysteresis experiments (open symbols) and showing remanence in field direction of the MPMS during warming from 5 to 300 K after measurement of NRM hysteresis loops (closed symbols). Values were normalized by sample weight as listed in Table 1. Additional sample plots in electronic supplement, Figs S6C, E, I, J.

Table 8. Comparisons of three different measurements at 5 K of zero-field remanence in $Am^2\ kg^{-1}$ parallel to the field direction (z) in the MPMS. (1) Average of upper limb (Mr+) and lower limb (Mr−) zero-field intercepts during hysteresis in fields of 5T (MrAv); (2) Upper limb zero-field intercept (Mr+) during reduction of field from +5 T (loop remanence) in NRM loop; (3) Zero-field intercept when +5 T field was turned off at end measurement of FC loop (postloop remanence); (4) Ratio of post-loop remanence (PLR) to loop remanence (LR).

Figure number and loop type		(1) MrAv	(2) Mr+ Loop Remanence	(3) Mr+ postloop Remanence	(4) Ratio PLR/LR
Fig. 3A	NRM	−0.01153	−0.00588	−0.00630	1.07
	FC	+0.02105	+0.0474	+0.0466	0.98
Fig. 3B	NRM	−0.00316	+0.00143	+0.000376	0.26[a]
	FC	+0.01243	+0.0425	+0.0412	0.97
Fig. 3C	NRM	−0.00594	−0.00101	−0.00104	1.03
	FC	+0.01807	+0.0514	+0.0504	0.98
Fig. 3D	NRM	−0.00361	−0.000929	−0.00116	1.25[a]
	FC	+0.01162	+0.0421	+0.0409	0.97
Fig. 3E	NRM	−0.00935	+0.00653	+0.00640	0.98
	FC	+0.03341	+0.0779	+0.0782	1.00
Fig, 3F	NRM	+0.00664	+0.0103	+0.00991	0.97
	FC	+0.01532	+0.0604	+0.0590	0.98
Fig. 3G	NRM	+0.02443	+0.0299	+0.0302	1.01
	FC	+0.05085	+0.0824	+0.0812	0.99
Fig. 3H	NRM	+0.00023	+0.00855	+0.00954	1.12
	FC	+0.01045	+0.0392	+0.0335	1.01
Fig. 3I	NRM	+0.00351	+0.0175	+0.0170	0.97
	FC	+0.01257	+0.0621	+0.0612	0.99
Fig. 3J	NRM	+0.00186	+0.0109	+0.0120	1.11
	FC	+0.01879	+0.0504	+0.0512	1.02

Note. [a]Only significant disagreements.

shift', even though ilmenite remanence and AF coupling govern internal details of the loops.

7 COOLING AND WARMING EXPERIMENTS

Part of the experimental procedure preceding and following the NRM and FC hysteresis loops at 5 K involved monitoring of the magnetization during cooling of the samples to 5 K and warming back to room *T*. The first step in all the experiments was to measure the parallel component of the NRM during cooling of the oriented sample before the initial 5 K hysteresis loop (Fig. 6, open symbols). After the NRM hysteresis loop at 5 K, the resultant remanent magnetization was measured with warming in ZF to room-*T* (Fig. 6, closed symbols). At the end of each NRM hysteresis loop the field was at +5 T, so the resulting remanence is approximately equivalent to that from a 5 K SIRM, with the caveat that the ilmenite remanence retains the polarity that it acquired on initial cooling. Thus the total remanence, probably including orientations of moments, was only moderately changed by the loop fields. At room *T*, a +5 T field was applied and maintained while the sample was cooled back to 5 K for the FC hysteresis loop. No record was made of the magnetization during this cooling. After the FC hysteresis loop, the field was removed and a second record of remanence was measured during warming to room *T* (Fig. 7).

7.1 NRM field-free cooling

The NRM field-free cooling curves in Figs 6 and S6, divide into two groups, based on NRM orientation in the MPMS. Those with the NRM oriented negatively in the instrument direction (Figs 6, A, B, D; S6C, S6E) show negative values, whereas those with the NRM oriented positively (Figs 6, F, G, H; S6I, S6J) show positive values. The NRM intensities measured in the cryogenic magnetometer at 300 K can be compared with the initial measurements in the MPMS instrument at 300 K, once the former are corrected trigonometrically for orientation in the instrument. The results in Table 2, with one exception, are comparable.

Samples with original negative NRM_Z (A–E), all show a gradual decrease in negative values (absolute increase) with cooling, and remain negative. Other features are extremely subtle. The curves for A, B, C flatten below 25 K, and D, E below 37 K. Sample C shows a slight dip 50–25 K, and E a slight dip between 50 and 37 K, that could relate to magnetization of ilmenite. Despite few distinctive features during cooling, all five NRM loops showed easily detected bimodal exchange bias with dominant positive peaks consistent with positive magnetization of ilmenite.

Samples with original positive NRM_Z (F to J), F, G show gradual decreases in positive values with cooling, and I, J weaker decreases though all stay positive. Sample H has a distinct Verwey transition, consistent with other experiments showing a trace of magnetite is present within the larger core from which this sample was taken. It shows an increase in magnetization with falling *T* unlike the other positive samples. Other features are extremely subtle. F, G, H, I, J all show subtle flattening near 50–60 K, probably related to the initial magnetization of ilmenite (T_N 57 K). Despite the lack of striking features during cooling, all five NRM loops showed easily detected bimodal exchange bias with dominant negative peaks consistent with magnetization of ilmenite, and presence of magnetite in H. Electronic supplement Section S7.1 and Table S1 contain a detailed evaluation of cooling results.

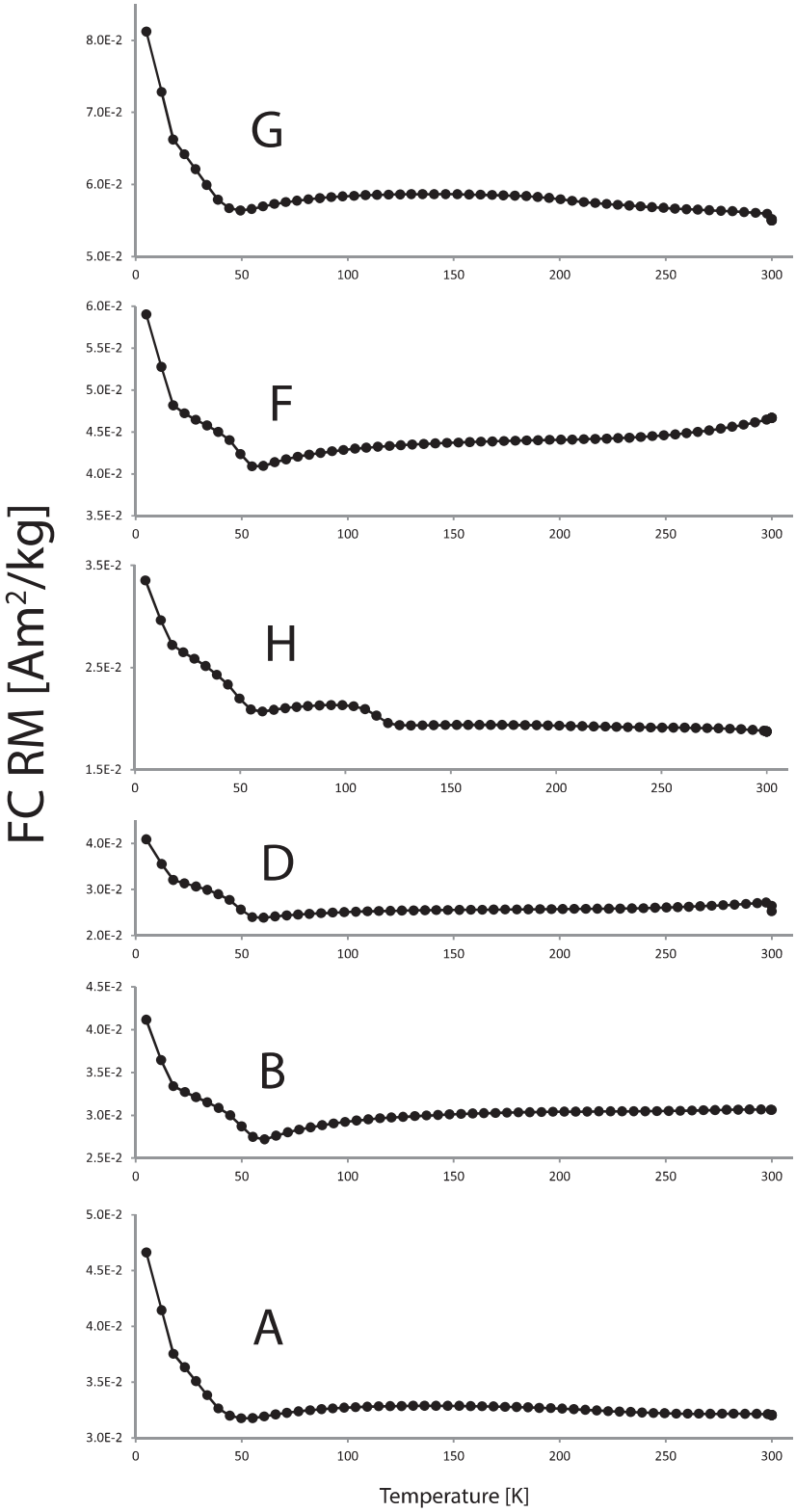

Figure 7. Plots showing remanence in the field direction of the MPMS during warming from 5 to 300 K after measurement of FC hysteresis loops. Values were normalized by sample weight as listed in Table 1. Additional sample plots are in electronic supplement Figs S7C, E, I, J.

7.2 Warming curves following NRM and FC loops

The warming curves measured after the initial NRM loops (Fig. 6) combined with the warming curves following the FC loops (Fig. 7) provide powerful insights into the nature of the magnetic materials and their interface coupling. Hysteresis loops ended at 5 K, with a +5 T field, and both sets of warming curves began at 5 K, after the field was removed. The initial remanence of each warming curve (postloop remanence) should be theoretically the same as the value Mr+ measured at 5 K in zero field on the upper limb of the relevant

hysteresis loop of Fig. 3. The single proviso for this is that Mr+ (loop remanence) measured during hysteresis involved gradual reduction of the field, whereas the value at the end of hysteresis (post-loop remanence) involved a sudden removal of the field. Table 8 shows that these two routes to remanence at 5 K, with two exceptions, give nearly identical results, which they should.

The effects in the warming curves are generally least subtle for those measured after the FC loops (Figs 7 and S7). The FC loops created a strong and highly oriented positive lamellar magnetism that, in turn, through AF coupling, created a negative magnetization in the ilmenite on passing through T_N. This negative ilmenite magnetization persists during the low-T hysteresis, creating a strong negative exchange bias. All the FC loops show a strong Mr+ on the upper limb of the hysteresis loop on return to zero field. This strong positive magnetization is interpreted as the lamellar magnetism held in place by the AF coupling with negatively magnetized ilmenite. The warming curves (Figs 7 and S7) have three parts in common. From 5 to 25 K there is sharp intensity drop, likely related to hardness of lamellar moments and AF coupling to ilmenite at lowest temperatures. The next interval 25–60 K shows another major drop, which we think is directly tied to loss of negative ilmenite magnetization. One might think this would cause an increase rather decrease in intensity, but we postulate that weakening of AF coupling allows the lamellar magnetism to become directionally more diverse and weaker, and in effect more influenced in orientation by the hematite host than by the adjacent ilmenite. Above 60 K there are few changes, except for the drop 112–125 K in Fig. 7H that clearly marks the Verwey transition for magnetite in this one sample.

The first group of NRM hysteresis loops (Figs 3 and S3, samples A–E) were produced by placing the NRM in the negative field direction of the MPMS, always producing bimodal exchange bias with the positive peak greater than the negative one (though in 3B the difference is small). Here again it is useful to examine the values of Mr+ on upper limbs of hysteresis loops at zero field in A–E, as follows: A-small negative, B-slight positive, C-negative, D-negative and E-positive. Thus, when these samples ended their residence in the strong positive field (with a strong positive lamellar magnetism), AF coupling with the predominant positive ilmenite magnetization (itself strongly maintained by the +5 T field), caused the lamellar magnetism to reverse immediately back toward its original predominantly negative orientation. Despite initial positive values for two curves, all five warming curves (Figs 6 and S6, A–E) move more negative (increasing negative magnetization or decreasing positive magnetization for S6E) with warming 5–25 K. Between 25 and 60 K effects are extremely subtle, unlike effects in warming after the FC loops. These are hard to link clearly to ilmenite, though AF coupling with positively magnetized ilmenite was lost here. However, weak effects could be attributed to the fact that the lamellar magnetisms here are coupled to ilmenite that is magnetized both positively and negatively. With further warming, A, C and D, all show an increase in negative magnetization. One speculates if these changes could be linked to a subtle removal of positive ilmenite magnetization at temperatures way above the traditional T_N (V. Shcherbakov, personal communication 2011). Curve B remains essentially flat and E shows a decrease in positive magnetization.

The second set of NRM hysteresis loops (Figs 3a and S3, samples F–J) were produced by placing the NRM in the positive field direction of the MPMS, always producing bimodal exchange bias with the negative peak greater than the positive one. The Mr+ values on upper limbs of hysteresis loops at zero field in F–J are all positive. These values are best explained in parallel with the positive values in the case of the FC loops, also with negative exchange bias, but here greatly weakened by the presence also of positive exchange bias. All five warming curves (Figs 6 and S6, F–J) show a sharp decrease in positive values with warming 5–25 K. Between 25 and 60 K all five curves show a basin-shape, again unlike effects in warming after the FC loops, but in a temperature range where ilmenite, both positively and negatively magnetized, is disordering. With further warming, F, G and I, all show an increase in positive magnetization possibly a signal of the removal at high T of negatively magnetized ilmenite. Samples H and J show little change, except for a very large drop in H, marking the Verwey transition in magnetite. The decrease at 120 K is larger than the equivalent drop in the warming curve after the FC loop possibly indicating a small amount of discrete (not coupled) MD magnetite.

7.3 Changes to room-*T* properties resulting from experiments

The end results of the two sets of warming curves provide an opportunity to study the magnetic changes to room-*T* lamellar magnetizations as the sample passed through two different processes. The first was the entire NRM loop process: field-free cooling (FF) from 300 to 5 K acquiring a strong ilmenite magnetization, then 5 T hysteresis, followed by FF warming to 300 K. The second process with FC: cooled in a +5 T field from 300 to 5 K, followed by a second 5 T hysteresis at 5 K, and then final FF warming to 300 K. This progression involves three different magnetizations measured at 300 K: NRM_Z, M_ZNRM and M_ZFC. Details of this progression in room-*T* properties are covered in electronic supplement Section S7.3.

8 CONCLUSIONS

Based on earlier measurements and theory concerning lamellar magnetism and low-T magnetic exchange bias in titanohematite with nano-scale ilmenite lamellae (McEnroe *et al.* 2007a), we developed a working model to predict the optimal orientation for placing the NRM within a magnetic instrument to obtain optimal measurements of magnetic exchange bias. This model involved ilmenite lamellae only 3–7 atomic layers (0.69–1.69 nm) thick, containing 1–3 Fe^{2+} layers and 2–4 Ti layers flanked by two 'contact layers'. Similarly very thin lamellae appear to predominate in the MOD22 samples based on EMP analyses, magnetic experiments, Mössbauer studies and TEM investigations summarized in Paper I.

Using cryogenic magnetometer measurements of the orientation of the NRM, each sample was strategically placed in an MPMS for hysteresis experiments. Here the original NRM was cooled in absence of a field down to 5 K before measurement. The hysteresis results on ten samples provided evidence for predominantly asymmetric bimodal exchange bias related to coupling of lamellar magnetism with the hard magnetization of ilmenite. These indicate that when the dominant NRM was oriented toward the positive field end of the MPMS, the dominant resulting exchange bias was negative. Conversely when the dominant NRM was oriented toward the negative field end of the MPMS, the dominant resulting exchange bias was positive. When the same samples were cooled in a field of +5 T from room-*T* down to 5 K, the lamellar magnetic moment was all reoriented to a positive direction before reaching T_N of ilmenite, and the result was a hard, negative ilmenite magnetization and consistent unimodal negative exchange bias.

The amounts of hysteresis shift were calculated in two ways: (1) By determining the height (peak) in $Am^2\ kg^{-1}$ of separation between the upper and lower limbs of the loops and then the peak location in T. (2) By determining the areas of separation between the upper and lower limbs of the loops, one area for unimodal loops and two areas for bimodal loops, and then determining the median field in T for each area. By (1) the largest shift for an FC loop was –0.694 T (3B). The largest shifts for larger peaks of NRM loops were +1.19 T (3B), +1.10 T (3D) and –1.04 T (3 G); but these shifts were exceeded by those of the smaller peaks –1.30 T (3B), –1.22 T (3D) and +1.10 T (3 G). The unusual bimodal loop for 3H has peak locations at –1.33 T and +1.31 T. By (2) the hysteresis shift is smallest for the field-cooled experiments, with a maximum value of –0.436 T (3 G). In results from NRM cooling, the shift is much larger for the separation with larger area of a bimodal loop, for example +1.47 T(3C) and +1.48 T(3D), but absolutely the largest in several cases, for example –1.64 T (3C) and –1.65 T (3D), for the separation with the smaller area of a bimodal loop. The unusual bimodal loop for 3H has mean field values of −1.68 and +1.64 T.

Note that in nearly all the bimodal loops the shifts based on area mean field values are larger than peak height field values, meaning that all the negative peaks have wide shoulders in a negative direction and all positive peaks have wide shoulders in a positive direction. This reflects hysteresis resistance to achievement of the exchange-biased state. A specific challenge in modeling is to explain why the hysteresis shifts measured in both ways are least in the FC loops, larger in the larger bimodal peaks in the NRM loops and largest of all in the smaller bimodal peaks in the NRM loops.

This sample behavior is consistent with development of very hard ilmenite magnetizations interior to nanoscale ilmenite lamellae at very low T. The ilmenite magnetizations, acquired on cooling through T_N of ilmenite, appear to have become and remain strongly constrained to original directions normal to (001) in fields of 5 T. The fact that magnetizations are approximately equal in fields +5 T and –5 T, suggests that unbalanced ilmenite magnetic moments within lamellae are very small. By contrast, the unbalanced moments of lamellar magnetism related to contact layers with hematite are relatively large, and in the same 5 T fields, these moments and those of adjacent hematite sublattices can be re-oriented extensively. Despite this, at intermediate fields, local AF coupling between ilmenite and contact layers with hematite provide examples of extreme magnetic exchange bias.

In addition to the two sets of hysteresis experiments on each of ten samples, records were made of magnetic intensity as the original NRM was cooled from 300 K down to 5 K before any hysteresis experiment, of intensity as each sample was warmed from 5 to 300 K after the NRM hysteresis experiments, and of intensity as each sample was warmed from 5 to 300 K after the FC hysteresis experiments. These provide background for further speculations about the magnetization processes. An interesting outcome was to learn that the remanence Mr+ (loop remanence), either positive or negative, measured at zero field during all NRM and FC hysteresis runs, was essentially identical to Mr+ measured immediately after a +5 T field was turned off (postloop remanence) at the end of each hysteresis experiment. With these many phenomena established, the next step is to develop comprehensive models to attempt to explain how this occurred.

ACKNOWLEDGEMENTS

This work was supported by Research Council of Norway grant 222666 to S. McEnroe. Assistance in the lab work at the IRM was provided by Amy Chen. The IRM is supported by the Instruments and Facilities Program, Earth Sciences Division, US National Science Foundation. Two anonymous reviewers are thanked for their detailed and constructive reviews.

REFERENCES

Fabian, K., McEnroe, S.A., Robinson, P. & Shcherbakov, V.P., 2008. Exchange bias identifies lamellar magnetism as the origin of the natural remanent magnetization in ilmeno-hematite from Modum, Norway, *Earth planet. Sci. Lett.,* **268**(3–4), 339–353.

Harrison, R.J., McEnroe, S.A., Robinson, P., Palin, E.J. & Kasama, T., 2007. The mechanism of giant exchange bias (>1 T) in a natural intergrowth of Fe_2O_3-$FeTiO_3$, *Phys. Rev. B,* **76,** 174436, doi:10.1103/PhysRevB.76.174436.

Harrison, R.J., McEnroe, S.A., Robinson, P. & Howard, C., 2010. Spin orientation in a natural Ti-bearing hematite: evidence for an out-of plane component, *Am. Mineral.,* **95,** 974–979.

Kasama, T. *et al.*, 2009. The application of Lorentz transmission electron microscopy to the study of lamellar magnetism in hematite-ilmenite, *Am. Mineral.,* **94,** 262–269.

Kato, H., Yamada, M., Yamauchi, H., Hiroyoshi, H., Takei, H. & Watanabe, H., 1982. Metamagnetic phase transitions in $FeTiO_3$, *J. Phys. Soc. Japan,* **51,** 1769–1777.

McCammon, C., McEnroe, S.A., Robinson, P. & Burton, B.P., 2009. Mössbauer spectroscopy used to quantify natural lamellar remanent magnetization in single-grains of ilmeno-hematite, *Earth planet. Sci. Lett.,* **288,** 268–278.

McEnroe, S.A., Carter-Stiglitz, B., Harrison, R.J., Robinson, P., Fabian, K. & McCammon, C.C., 2007a. Magnetic exchange bias of more than 1 Tesla in a natural mineral intergrowth, *Nat. Nanotechnol.,* **2,** 631–634.

McEnroe, S.A., Robinson, P., Langenhorst, F., Frandsen, C., Terry, M.P. & Boffa Ballaran, T., 2007b. Magnetization of exsolution intergrowths of hematite and ilmenite: mineral chemistry, phase relations, and magnetic properties of hemo-ilmenite ores with micron- to nanometer-scale lamellae from Allard Lake, Quebec, *J. geophys. Res.,* **112**(B10), doi:10.1029/2007JB004973.

McEnroe, S.A., Robinson, P., Miyajima, N., Fabian, K., Dyar, D. & Sklute, E., 2016. Lamellar magnetism and exchange bias in billion-year-old titanohematite with nanoscale ilmenite exsolution lamellae: I. Mineral and magnetic characterization, *Geophys. J. Int.,* **206,** 470–486.

Robinson, P., Harrison, R.J., McEnroe, S.A. & Hargraves, R., 2002. Lamellar magnetism in the hematite-ilmenite series as an explanation for strong remanent magnetization, *Nature,* **418,** 517–520.

Robinson, P., Harrison, R.J., McEnroe, S.A. & Hargraves, R., 2004. Nature and origin of lamellar magnetism in the hematite-ilmenite series, *Am. Mineral.,* **89,** 725–747.

Robinson, P., Fabian, K., McEnroe, S.A. & Heidelbach, F., 2012. Influence of lattice-preferred orientation with respect to magnetizing field on intensity of remanent magnetization in polycrystalline hemo-ilmenite, *Geophys. J. Int.,* **192**(2), 514–536.

SUPPORTING INFORMATION

Supplementary data are available at *GJIRAS* online.

Section S7.1 Details of NRM field–free cooling

Section S7.3 Details of progression of room–T properties during experiments

Figures S3. NRM and FC hysteresis loops for all ten samples. (For convenience cross references are only to S3 figures)

Figure S3A. (NRM) Positive NRM placed 48.3° from negative direction of MPMS, equally 'favorable' as 42.6° in Fig. S3F and 43.4° in Fig. S3I. Loop closures: −2.75 T, +2.63 T. Smaller loop separation at −1 T 0.017 $Am^2\ kg^{-1}$, larger loop separation at +1 T 0.038 $Am^2\ kg^{-1}$. Bimodal with positive side greatly predominant. An almost exact twin of Fig. S3G where negative side

predominates. This provides insight into the history of lamellar magnetization. Both pieces are from the same MOD–22–6 sample from material that undoubtedly cooled and exsolved at the same T, with a similar orientation to the Proterozoic magnetizing field. Thus, the main difference concerns negative (here) versus positive (Fig. S3G) placement in the MPMS! (**FC**) Predicted negative exchange bias. Loop closures: 1.88 T and +1.88+ T. Maximum loop separation at −0.19 T 0.076 Am^2 kg^{-1}. The different shapes of S3A and S3G could relate to the fact that, in order to achieve this negative exchange bias in S3A, all the dominant negative lamellar remanence had to be overcome during field cooling in a positive field above TN of ilmenite. By contrast, in the example of S3G, only the subordinate negative lamellar remanence had to be overcome.

Figure S3B. (NRM) Negative NRM placed 27° from negative direction of MPMS. Loop closures: −4.5 T and +4.35 T. Smaller loop separation at −1.30 T 0.034 Am^2 kg^{-1}, larger loop separation at +1.188T 0.040 Am^2 kg^{-1}. Bimodal with positive side predominant. (**FC**) Predicted negative exchange bias. Loop closures: −4.25 T, +4.63 T. Maximum loop separation at −0.694 T 0.069 Am^2 kg^{-1}.

Figure S3C. (NRM) Positive NRM placed 71.8° from the negative direction of the MPMS. Apparent loop closures: −5 T and +5 T. Smaller loop separation at −1.19T 0.024 Am^2 kg^{-1}, larger loop separation at +1.08 T 0.032 Am^2 kg^{-1}. Bimodal with positive side predominant. (**FC**) Predicted negative exchange bias. Apparent loop closures: − 5 T, +5 T. Maximum loop separation at −0.30 T 0.081 Am^2 kg^{-1}.

Figure S3D. (NRM) Positive NRM placed 71.8° from the negative direction of the MPMS the same as Fig. A3c. Apparent loop closures: −5 T and +5 T. Smaller loop separation at −1.22T 0.023 Am^2 kg^{-1}, larger loop separation at +1.104 T 0.030 Am^2 kg^{-1}. Bimodal with narrow center. Positive side predominates. (**FC**) Predicted negative exchange bias. Apparent loop closures: − 5 T, +5 T. Maximum loop separation at −0.541 T 0.065 Am^2 kg^{-1}.

Figure S3E. (NRM) Negative NRM placed 11.4° from the positive direction of the MPMS, far from favorable orientations for Figs 3a, 3i, 3j. Loop closures: −1.5 T and +1.38 T. Smaller loop separation at −0.50 T 0.028 Am^2 kg^{-1}, larger loop separation at +0.48 T 0.041 Am^2 kg^{-1}. Bimodality not easy to see, but positive side predominates. Despite unfavorable orientation, provides another example of positive exchange bias with negative placement of NRM. (**FC**) Though unimpressive, it is another convincing example of predicted negative exchange bias. Loop closures: −1 T, +0.35 T. Maximum loop separation at −0.16 T 0.014 Am^2 kg^{-1}.

Figure S3F. (NRM) Negative NRM placed 42.6° from negative direction of MPMS. Loop closures: −3.8 T and +3.55 T. Larger loop separation at −0.98 T 0.056 Am^2 kg^{-1}, smaller loop separation at +1.08 T 0.038 Am^2 kg^{-1}. Strikingly bimodal with larger negative loop separation demonstrating that the dominant component of NRM, as placed positive in the MPMS, is stronger than the negative component. In all earlier 'unoriented' measurements, we had never found a sample providing an NRM loop with negative exchange bias. Was this just by chance, or was there a deeper explanation? The first 'oriented' experiments, Figs S3F, S3G and S3I, answered the question. (**FC**) Predicted negative exchange bias. Loop closures: −2.25 T, +3.0 T. Maximum loop separation at −0.57 T 0.081 Am^2 kg^{-1}. The central loop separation looks higher than in Fig. S3I because the vertical scale is more than doubled.

Figure S3G. (NRM) Negative NRM placed 35.1° from the positive direction of the MPMS, less favorable than 43.4 and 42.6° for Figs S3I and S3F. This has the strongest NRM of all samples (Table 2). Loop closures: −2.9 T and +2.25 T. Larger loop separation at −1.04 T 0.082 Am^2 kg^{-1}, smaller loop separation at +1.10 T 0.030 Am^2 kg^{-1}. Bimodal loop with negative side greatly predominant. This the most convincing example of negative exchange bias with positive placement of the NRM, yet more striking taking into account the smaller vertical scale compared to Fig. S3F. The more asymmetric bimodality is consistent with an NRM neither parallel nor normal to the instrument field. (**FC**) Predicted negative exchange bias. Loop closures: −2.1 T, +2.13 T. Maximum loop separation at −0.28 T 0.133 Am^2 kg^{-1}.

Figure S3H. (NRM) Positive NRM placed 76.6° from the positive direction of the MPMS. Loop closures: −4.9 T and +4.7 T. Larger loop separation at −1.33T 0.031 Am^2 kg^{-1}, smaller loop separation at +1.31 T 0.023 Am^2 kg^{-1}. Loop is bimodal. Remarkable feature is steep central slope, both in this and in the FC loop, over the range +0.2 T to −0.2 T. Represents a small fraction of magnetite, probably multi−domain, not coupled to titanohematite, that was strongly magnetized below the Verwey transition. This is also shown in the NRM loop by a very small central peak. Outside the central region the negative side predominates, thus another convincing example of a negative exchange bias. (**FC**) Predicted negative exchange bias. Loop closures: −4.25 T, +4.75 T. Maximum loop separation at −0.59 T 0.045 Am^2 kg^{-1}.

Figure S3I. (NRM) Positive NRM placed 43.4° from the positive direction of the MPMS. Loop closures: −3.3 T and +3.25 T. Larger loop separation at −1.09 T 0.038 Am^2 kg^{-1}, smaller loop separation at +1.09 T 0.028 Am^2 kg^{-1}. NRM loop is mildly bimodal, with negative exchange bias predominant. (**FC**) Predicted negative exchange bias. Loop closures: −1.85 T, +2.05 T. Maximum loop separation at −0.10 T 0.111 Am^2 kg^{-1}.

Figure S3J. (NRM) Positive NRM placed 54.8° from the positive direction of the MPMS. Loop closures: −2.125 T and +1.4 T. Larger loop separation at −0.583 T 0.023 Am^2 kg^{-1}, smaller loop separation at +0.585 T 0.019 Am^2 kg^{-1}. Loop is barely bimodal, so thin that it could only be shown using a vertical exaggeration x20. (**FC**) Loop slightly better with predicted negative exchange bias. Loop closures: −1.35 T, +0.4 T. Maximum loop separation at −0.146 T 0.089 Am^2 kg^{-1}.

Figure S4 The remanent hysterestic curves 'Mrh'(B) used in preparing shaded curves in Figs 3 and S3A−S3J, and in obtaining various values in tables (see Fig. 4 for details).These quantify the vertical half−height of the loop separation at each field value: Mrh(B) = (M + (B) − M−(B))/2 (the full vertical height of the loop loop separation always exactly double this). For the NRM loops, the 'Mrh curves are clearly bimodal with two peaks in which one is dominant. Most peaks are skewed with a flatter slope on the high field side. For the FC loops, the Mrh curves are generally unimodal and commonly flat–topped. Steep and flat slopes follow no clear pattern.

Figure S6 Sample plots for C, E, I, J showing the magnetization in the field direction of the MPMS during FF cooling 300 to 5 K before NRM hysteresis experiments (open symbols) and showing remanence in field direction of the MPMS during warming from 5 K to 300 K after measurement of NRM hysteresis loops (closed symbols).

Figure S7 Sample plots for C, E, I, J showing remanence in the field direction of the MPMS during warming from 5 K to 300 K after measurement of FC hysteresis loops.

Table S1. Comparisons of four different measurements (bold) in [Am^2 kg^{-1}] of zero–field remanence parallel to the field direction (z) in the MPMS. (1) NRM at 300 K (NRM_z); (2) Magnetization at 5 K before application if any magnetic field (Mz 5 K), (3) Change in magnetization caused by cooling of the NRM from 300 K to 5 K without application of any field (NRM_z – Mz 5 K). (4) Change

factor NRM_z to Mz 5 K. (5) Average of upper limb (Mr+) and lower limb (Mr–) zero–field intercepts during NRM hysteresis in fields of 5 T at 5 K (Mr AvNRM); (6) Change in magnetization at 5 K caused by NRM hysteresis in fields of 5 T (Mz 5 K –MrAvNRM); (7) Change factor Mz 5 K to MrAvNRM. (8) Average of upper limb (Mr+) and lower limb (Mr−) zero–field intercepts during FC hysteresis in fields of 5 T at 5 K (MrAvFC); (9) Change in magnetization at 5 K caused by FC hysteresis in fields of 5 T (MrAvFC –MrAvNRM); (10) Change factor MrAvNRM to MrAvFC. Adjusted where MrAvNRM negative. (11) Change in magnetization at 5 K caused by FC hysteresis in fields of 5 T (Mr AvFC –Mz 5 K); (12) Change factor Mz 5 K to MrAvFC. Adjusted where Mz 5 K negative.

Table S2. Comparisons of three different measurements (bold) in $Am^2\ kg^{-1}$ of zero–field remanence all at 300 K parallel to the field direction (z) in the MPMS. (1) NRM (NRM_z) at beginning of experiments. (2) Magnetization after warming from 5 K following NRM hysteresis loop. (MzNRM), (3) Change in magnetization caused by the entire NRM loop process from original NRM_z to MzNRM. (4) Change factor NRM_z to MzNRM. (5) Magnetization after warming from 5 K following FC hysteresis loop. (MzFC), (6) Change in magnetization caused by the FC loop process from MzNRM to MzFC (7) Change factor MzNRM to MzFC. Adjusted where MzNRM negative. (8) Change in magnetization caused by the combined NRM loop and FC loop processes from original NRM_z to MzFC. (9) Change factor MrFC/NRM_z. Adjusted where NRM_z negative.

Please note: Oxford University Press is not responsible for the content or functionality of any supporting materials supplied by the authors. Any queries (other than missing material) should be directed to the corresponding author for the paper.